

Accepted Manuscript

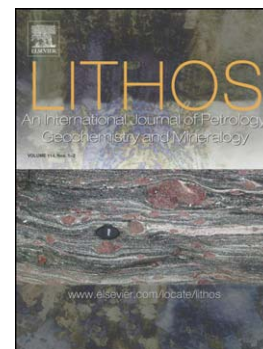
Age, Origin, and Thermal Evolution of the ultra-fresh 1.9 Ga Winnipegosis Komatiites, Manitoba, Canada

Pedro Waterton, D. Graham Pearson, Bruce Kjarsgaard, Larry Hulbert, Andrew Locock, Steve Parman, Bill Davis

PII: S0024-4937(16)30373-5
DOI: doi:[10.1016/j.lithos.2016.10.033](https://doi.org/10.1016/j.lithos.2016.10.033)
Reference: LITHOS 4131

To appear in: *LITHOS*

Received date: 7 July 2016
Accepted date: 26 October 2016



Please cite this article as: Waterton, Pedro, Pearson, D. Graham, Kjarsgaard, Bruce, Hulbert, Larry, Locock, Andrew, Parman, Steve, Davis, Bill, Age, Origin, and Thermal Evolution of the ultra-fresh 1.9 Ga Winnipegosis Komatiites, Manitoba, Canada, *LITHOS* (2016), doi:[10.1016/j.lithos.2016.10.033](https://doi.org/10.1016/j.lithos.2016.10.033)

This is a PDF file of an unedited manuscript that has been accepted for publication. As a service to our customers we are providing this early version of the manuscript. The manuscript will undergo copyediting, typesetting, and review of the resulting proof before it is published in its final form. Please note that during the production process errors may be discovered which could affect the content, and all legal disclaimers that apply to the journal pertain.

Age, Origin, and Thermal Evolution of the ultra-fresh ~1.9 Ga**Winnipegosis Komatiites, Manitoba, Canada**

^aPedro Waterton, ^aD. Graham Pearson, ^bBruce Kjarsgaard, ^{b*}Larry Hulbert, ^aAndrew Locock, ^cSteve Parman,

^bBill Davis

a. Earth and Atmospheric Sciences Department, University of Alberta, Edmonton, Alberta, Canada.

T6G 2E3. email: waterton@ualberta.ca, gdpearso@ualberta.ca, alocock@ualberta.ca

b. Geological Survey of Canada, 601 Booth St., Ottawa, ON, Canada. K1A 0E8. email:

bruce.kjarsgaard@canada.ca, bill.davis@canada.ca

*Present Address. NiPtx Inc. 262 Cranleigh Place S.E., Calgary, Alberta, Canada. T3M 0N5. email:

lhlhulbert7@gmail.com

c. Department of Earth, Environmental and Planetary Sciences, Brown University, Box 1846, 324 Brook

Street, Providence, Rhode Island 02912. U.S.A. stephen_parman@brown.edu

Abstract

The Proterozoic spans the longest portion of Earth's history, yet in contrast to the Archaean, the record of komatiites and related high MgO igneous rocks from this Eon is sparse. This paper describes the pristine Palaeoproterozoic Winnipegosis Komatiites, from Manitoba, Canada, which form part of the Circum-Superior Belt large igneous province. We present a comprehensive petrographical investigation, mineral and bulk rock geochemistry, and Al-in-olivine thermometry for the Winnipegosis Komatiites, along with new U-Pb SHRIMP dating of zircons from a mafic unit, which yield an age of 1870.3 ± 7.1 Ma for the Winnipegosis Komatiite Belt. The komatiites are Al-undepleted and dominated by massive olivine porphyritic flows with a median thickness of 6 m. Differentiated flows containing layers of olivine spinifex are present, but rare. Trace element data indicate the komatiites were derived from depleted mantle, and subsequently contaminated with 2 – 3% continental crust. Temperatures from Al-in-olivine thermometry are consistent with a nominally dry melt, and combined with olivine-melt Mg-Fe partitioning, suggest a parental melt with ~24 wt% MgO and a liquidus (olivine) temperature of ~1501 °C, approximately 100 °C cooler than their hottest Archaean counterparts. At ~1424 °C chromite joined olivine as a crystallising phase. Olivine and chromite phenocrysts were re-mixed with residual melt shortly before or during komatiite eruption, which occurred by the time the magma had cooled to ~1321 °C. Combined geochemical and geological evidence requires that the Winnipegosis Komatiites erupted onto rifting continental crust. Their high liquidus temperatures require anomalously hot mantle. Considering the Winnipegosis Komatiites in the context of the broader Circum-Superior Belt, we suggest that these magmas formed from a mantle plume that was deflected towards the margins of the Superior craton by strong gradients in lithospheric thickness. This interpretation of the mode of formation of the Circum-Superior Belt casts doubt on ambient mantle potential temperatures as high as 1600 °C during the Proterozoic.

1. Introduction

Komatiites are generally believed to represent high-temperature, large-degree melts of the mantle (Nisbet et al. 1993; Arndt et al. 2008). As such, they have long been used as probes of both the chemical and thermal evolution of the mantle through time (Bickle et al. 1976; Maier et al. 2009; Campbell & Griffiths 2014). However, the temporal record of mantle temperature and chemistry provided by komatiites is irregular; the vast majority of komatiites erupted during the Archaean (Arndt et al. 2008), with only two occurrences known from the Phanerozoic (Echeverria 1980; Hanski et al. 2004). Despite comprising almost half of Earth history, only a handful of komatiites and related high MgO igneous rocks have been reported from the Proterozoic Eon, including: Ti-rich komatiites of the Karasjok and Central Lapland Greenstone Belts (Barnes & Often 1990; Hanski et al. 2001); basaltic komatiites of the Vetreny Belt, (Puchtel et al. 1997); and a number of basaltic komatiites and compositionally similar intrusions from the Circum-Superior Belt (Arndt 1982; Arndt et al. 1987; Hynes & Francis 1982; Minifie et al. 2013).

In light of the paucity of Proterozoic komatiites, this paper describes the exceptionally fresh ~1.87 Ga Winnipegosis Komatiites from Manitoba, Canada. The minimally altered nature of the Winnipegosis Komatiite sequence provides an excellent opportunity both to study komatiite formation during the Proterozoic, and to compare the chemical and thermal state of Archaean and Proterozoic mantle. We present petrographical and geochemical observations with a view to understanding the mode of formation and thermal evolution of the Winnipegosis Komatiites. We demonstrate that the Winnipegosis lavas are komatiites by any definition, showing spinifex textures and derivation from a liquid with > 18 wt% MgO (Kerr & Arndt 2001). The Winnipegosis Komatiites show many geochemical similarities to Archaean Al-undepleted komatiites, and formed from a nominally dry, depleted mantle source. Their high liquidus temperatures are ~100 °C lower than their hottest Archaean counterparts, but still require thermally anomalous mantle for their formation. We discuss possible modes of formation of the Winnipegosis Komatiites in light of these findings and the regional geological context.

2. Geological Setting

The Winnipegosis Komatiite Belt (WKB; Hulbert et al. 1994) is located in the Superior Boundary Zone, in Manitoba, Canada, adjacent to the subsurface extension of the Thompson Nickel Belt (Figure 1). The Superior Boundary Zone lies along the northwestern margin of the Archaean Superior Craton, and forms a narrow eastern foreland to the ~1.8 Ga Trans-Hudson Orogen (e.g White et al. 2002). The Trans-Hudson Orogen was formed during the closure of the Manikewan Ocean (Stauffer 1984), and resulted in the juxtaposition of the Superior Craton with the amalgamated Rae and Hearne Cratons, and a number of continental fragments including the Archaean – Palaeoproterozoic Sask Craton (Lucas et al. 1993; Corrigan et al. 2009). Closure of the Manikewan Ocean is believed to have begun by 1915 Ma, as evidenced by the oldest oceanic arc rhyolites in the juvenile portion (Reindeer Zone) of the Trans-Hudson Orogen (Baldwin et al. 1987). However, arc-related rocks are not apparent along the western Superior margin until the ca. 1.89 Ga initiation of magmatism in the Snow Lake Arc, interpreted as a pericratonic arc outboard of the Superior Boundary Zone on the basis of negative ϵ_{Nd} and inherited Archaean zircon grains (David et al. 1996; Percival et al. 2005; Corrigan et al. 2009).

Bimodal mafic/ultramafic and felsic magmatism within the Thompson Nickel Belt at ca. 1.88 Ga (Hulbert et al. 2005; Heaman et al. 2009) and mafic/ultramafic magmatism in the WKB at ca. 1.87 Ga (Section 2.2) are contemporaneous with ongoing magmatism in the Snow Lake Arc and continued closure of the Manikewan Ocean, implying their formation along a convergent margin (Corrigan et al. 2009; Heaman et al. 2009). The Thompson Nickel Belt and WKB also form part of a ~3000 km long ca. 1.88 Ga bimodal magmatic system that wraps around the northern and western margins of the Superior Craton, known as the Circum-Superior Belt (CSB; Baragar & Scoates 1981). The CSB is considered a Large Igneous Province (LIP; Ernst & Bleeker 2010), though interpretations of its mode of formation are divided (e.g. Heaman et al. 2009; Minifie et al. 2013).

Arc magmatism and associated sedimentation continued in the juvenile Reindeer Zone of the Trans-Hudson

Orogen until ca. 1.82 Ga (Machado et al. 1999; Hollings & Ansdell 2002), before the terminal collision of the Superior craton with the Rae, Hearne and amalgamated terranes at ca. 1.83 – 1.80 Ga (Ansdell et al. 1995; Corrigan et al. 2009).

2.1 The Winnipegosis Komatiite Belt

The WKB lies beneath 120 – 500m of Palaeozoic cover (McGregor 2011), and was first identified as a ~150 x 30 km linear magnetic high in the southern, subsurface extension of the Superior Boundary Zone, centred beneath Lake Winnipegosis (Hulbert et al. 1994). During the 1990s Cominco drilled 27 geophysical targets within the belt as part of an exploration program for Thompson Nickel Belt style Ni-Cu deposits (McGregor 2011). The magnetic high was found to comprise a greenstone belt dominated by tholeiitic basalt and komatiite, intercalated with subordinate carbonate and shale sediments (Figure 1c). These overlie a thin interval of discontinuous basal conglomerate and sandstone, which rests unconformably on Superior Craton tonalite dated at 2792 ± 1.6 Ma in borehole RP92-5. Lava flow-tops dip consistently to the West. A single borehole (RP92-8) intersected further basaltic rocks structurally up-section from the komatiites. However, it is not certain whether this represents a stratigraphically distinct unit or a thrust repetition of the sequence (Burnham et al. 2009; McGregor 2011). The entire belt has undergone sub-greenschist to greenschist facies metamorphism, which likely occurred during the terminal collision phase of Trans-Hudson Orogeny. The lower degree of metamorphism and deformation in the region of the WKB compared to the Thompson Nickel Belt has previously been ascribed to the WKB's position in a re-entrant adjacent to the Thompson promontory (White et al. 2002; Ansdell 2005).

2.2 Revised age of the Winnipegosis Komatiite Belt

Coarse-grained basalt from borehole RP92-4, representing either a thick flow or sill (Burnham et al. 2009), yielded a U-Pb TIMS zircon age initially interpreted as $1864 +6/-4$ Ma (Hulbert et al. 1994). However, our re-analysis of the original data found that the precision suggested by this age is overly optimistic, and we

instead prefer an age of ca. 1860 – 1890 Ma. A second appraisal of the zircons isolated by Hulbert et al. (1994) identified whole crystals and fragments of prismatic igneous zircon with sharp crystal edges, ~50 – 200 μm in size. Backscattered electron (BSE) images reveal broad, faint igneous zoning in some grains. However, the zircons are heavily fractured, and many show mottled and irregular dark patches in BSE, indicative of metamictisation and alteration. To avoid these altered domains, we attempted a re-measurement of the age of the zircons by Sensitive High Resolution Ion MicroProbe (SHRIMP). A weighted average $^{207}\text{Pb}/^{206}\text{Pb}$ age of 14 points with <5% discordance yields 1870.3 ± 7.1 Ma (95% confidence limits), which overlaps within error, but is slightly older than the previous age determination (see Supplementary Information for details).

3. Petrography and flow descriptions

Thin sections from approximately 200 samples from a 250 m section of komatiite intersected by borehole RP91-1A (hereafter RP1A), and approximately 70 samples from a 230 m section of komatiite intersected by borehole RP94-12 (hereafter RP12) were investigated petrographically. Previous core logging and petrographical examination of RP1A (Hulbert et al. 1994) identified at least 28 komatiite flows ranging between ~3 m and ~36 m in thickness, with a median thickness of 6 m. Core logging of RP12 (McGregor 2011) did not divide the komatiite section into flows, but noted a prominent spinifex horizon towards the top of the borehole.

3.1 Massive flows

Massive olivine porphyritic flows comprise all of the flows intersected by RP1A, and the majority of flows in RP12. Olivine and chromite comprise the only phenocryst phases, and are relatively evenly distributed throughout the depth profile of each flow. There is no large-scale settling of olivine to form a cumulate layer, and no spinifex textures are observed. Olivine phenocrysts most commonly occur as subhedral, equant grains typically 0.1 – 2 mm in length, which may be fractured or rounded and show skeletal overgrowths (Figures 2a, b, c). Olivine also forms large (up to ~10 mm) semi-skeletal grains with large embayments. Chromite is found as euhedral microphenocrysts typically <200 μm across, and commonly forms 3 – 100 μm euhedral to rounded inclusions within olivine phenocrysts (Figure 2a). Clinopyroxene, devitrified glass, and pseudomorphs after olivine can be found as groundmass phases throughout, though their size and habit varies significantly with depth in each flow. A typical sample from near the base of a flow is shown in Figure 2b. Chill margins are identifiable by their 'web' of pseudomorphosed chain olivine dendrites, isolating pockets of dendritic or spherulitic cpx, and contain ~5 - 20 vol% olivine phenocrysts (Figure 2c).

3.2 Differentiated flows

One strongly differentiated flow, >6.7 m thick, is recognised in borehole RP12, with characteristics similar to those observed in komatiites from Gilmour Island (Arndt 1982). The upper chill margin is similar to those seen in the massive flows, but appears to grade over ~0.5 m into a phenocryst-free olivine spinifex zone (Figure 2d), containing cruciform chromite typical of spinifex-textured komatiites (Barnes 1998). Less than 1.2 m below the base of this olivine spinifex zone is a >1 m layer of acicular – subhedral pyroxene phenocrysts < 4 mm in length, set in a matrix of pyroxene and plagioclase. The lowermost sample obtained from this flow (<3.2 m from the base of the acicular pyroxene layer) contains large (~10 mm) hopper olivine crystals set in a matrix of clinopyroxene dendrites and glass. Though we lack samples from the base of the flow, core logging (McGregor 2011) indicates the presence of an olivine cumulate with approximately 40% olivine below the hopper olivine layer.

Two more olivine spinifex layers are recognised in RP12, but both are underlain (within <10 m) by samples similar to those from the massive flows. It is inferred that these represent thinner differentiated flows and/or flows which did not fully differentiate.

3.3 Alteration and metamorphism

Samples from borehole RP1A are generally excellently preserved, with approximately one third of samples retaining $\geq 70\%$ fresh olivine phenocrysts. A few samples show virtually no breakdown of phenocrystic olivine except along serpentinised cracks. However, as reported in previous studies of komatiite (Parman et al. 1997), some areas of apparently fresh olivine are zoned with Fe increasing towards serpentinised cracks rather than the original crystal edges (Figure 3). We interpret this as a metamorphic effect, due to diffusion of Fe into the olivine and/or diffusion of Mg out of the olivine during serpentinisation. Groundmass olivine is pervasively altered to talc and serpentine, but clinopyroxene appears stable in most samples, with preservation of even the finest pyroxene dendrites and spherulites. Chromite appears unaltered in most samples, but phenocrysts may show magnetite overgrowths (Arndt & Lesher 1992). Metamorphism is

largely restricted to hydration along cracks and veins, and the metamorphic assemblage of serpentine, talc, chlorite and magnetite (plus pyroxene) corresponds to the prehnite-pumpellyite facies of Jolly (1982). Complete destruction of primary igneous mineralogy is only observed adjacent to large carbonate veins.

Samples from borehole RP12 are generally more altered, with many samples retaining little or no olivine. Though some samples appear to preserve up to 80% of phenocrystic olivine, these olivine crystals may have a 'mottled' appearance and contain tiny unidentified metamorphic grains suggesting their incipient breakdown. The metamorphic assemblage consists of chlorite, tremolite-actinolite, talc, and magnetite. Although pyroxene is preserved in most samples, it is occasionally replaced by tremolite-actinolite, indicative of lower greenschist facies (Jolly 1982).

4. Methods

4.1 Sample selection for geochemistry

A large body of core samples, rock powders, and thin sections, from >250 samples used during the initial characterisation of the rocks by both Cominco and the Geological Survey of Canada (GSC), was obtained from the GSC archives in Ottawa. We utilised a large database (hereafter the 'GSC database') of unpublished geochemical data collected during the 1990s, including whole rock major element data measured by XRF; whole rock $\text{Fe}_2\text{O}_3:\text{FeO}$, H_2O_t , and CO_2 determined by wet chemical methods; and mineral analyses by EPMA (Supplementary Data).

Samples chosen for re-analysis were screened to exclude those with ≥ 0.3 wt% CO_2 and high H_2O_t , as these likely represent those most affected by the formation of carbonate and talc-serpentine veins, and hence fluid flow during metamorphism. Based on this screening, and attempting to maintain a large range in both MgO contents and stratigraphic position, a subset of 20 komatiite samples from borehole RP1A and 14 komatiite samples from RP12 were chosen for new geochemical analysis.

4.2 Whole rock major and trace elements

Whole rock major and minor element geochemistry was measured by X-ray fluorescence (XRF) on $\text{Li}_2\text{B}_4\text{O}_7$ fusion disks at Franklin and Marshall College (Mertzman 2000). Ten replicates of the OKUM (Ontario komatiite) certified reference material (CRM) were measured to assess the repeatability under measurement conditions (Jcgm 2008, hereafter 'repeatability') and accuracy of the method. Most major and minor elements were repeatable to a precision of $< 2\%$ ($1\sigma_{\text{relative}}$); K_2O , P_2O_5 , and V, present in low concentrations in OKUM, had repeatabilities of $< 5\%$. Loss on ignition (LOI) was variable, with a repeatability of $\sim 8\%$. All elements except Cr overlap with the certified values (IAG 2015) within 95% confidence limits, and we therefore consider them accurate at the level of precision of the measurements. Chromium is about 5% (relative) lower than the certified values, and lies just outside the 95% confidence limits.

Trace elements, including rare earth elements (REEs), were measured following a procedure similar to Ottley et al. (2003) at the Arctic Resources Geochemistry Laboratory at the University of Alberta. A mass of 0.1 ± 0.01 g of rock powder per sample was dissolved in Savillex PFA beakers with 4 mL of concentrated HF (28.7 M) and 1 mL of concentrated HNO_3 (15.4 M, both acids Teflon distilled in-house) and refluxed on a hotplate at 150 °C for >120 hours. Due to incomplete dissolution of some samples at this stage, all samples were dried down and again refluxed in 2 mL of concentrated HF and 2 mL concentrated HNO_3 at 150 °C for >120 hours, after which all samples appeared fully dissolved. Samples were then dried down before being evaporated to near dryness three times in concentrated HNO_3 , and diluted in 3% HNO_3 for measurement. Most trace elements were analysed at a mass resolution of 300 (10% peak-valley definition) on a Nu Atom ICP-MS, with the exception of the transition metals (Sc, Cr, Co, Ni, Cu), which were measured on an Element 2 ICP-MS at a mass resolution of 4000.

Twelve dissolutions of the OKUM CRM were measured to monitor repeatability and accuracy. All REEs, Rb, Sr, and Y were repeatable to $\leq 2\%$ ($1\sigma_{\text{rel}}$) over 3 analytical sessions. The elements Cs, Ba, Hf, Th, and U had repeatabilities of <4%; Zr and Pb had repeatabilities of $\sim 7\%$. All elements overlap with the certified values within 95% confidence limits, and are therefore deemed accurate at the level of precision of the analyses. However, we note that Zr in our measurements is about 7% below the certified value, despite the agreement within confidence limits. Transition metal analyses were repeatable to $\sim 3\%$ ($1\sigma_{\text{rel}}$), with Sc, Co, Ni, and Cu overlapping with certified values within 95% confidence limits. Cr data measured by ICP-MS was systematically high compared to both the certified OKUM value and XRF data from this study, likely due to an uncorrected interference during measurement, and is not used further as it is both less repeatable and less accurate than the data measured by XRF. However, it shows a strong correlation with the XRF data (Supplementary Information), which we interpret as evidence that chromite was fully dissolved in both the OKUM standard and Winnipegosis samples.

4.3 Mineral EPMA analyses

Major, minor, and trace element compositions of fresh olivine and co-existing olivine-chromite pairs from thin sections of the Winnipegosis Komatiite, were analysed using a JEOL 8900R electron microprobe at the University of Alberta. These measurements can be divided into 'routine' measurements performed to obtain major element compositions only, and 'high precision' measurements designed to measure trace elements, in particular for the application of the Al-in-olivine - spinel thermometer (Wan et al. 2008; Coogan et al. 2014). Routine measurements were performed with peak measurement times of 30 s for most elements using a beam current of 20 nA. High precision measurements were carried out using a beam current of 100 nA, and much longer analysis times. Aluminium was measured for 240 s on peak, with upper and lower backgrounds of 120 s each. These conditions yielded an average limit of detection of 0.0019 wt% Al_2O_3 (10 ppm Al), with the Potts (1992, p.11) limit of determination (blank + 6σ) at 0.0039 wt% Al_2O_3 (21 ppm Al). All measurements used an accelerating voltage of 20 kV.

Due to the lack of a CRM for trace elements in olivine, we report data from two different in-house San Carlos olivine standards to assess the precision and the accuracy of the method. The first, SC-BK, was characterised by LA-ICP-MS to have an Al-content of 80.4 ± 2.3 ppm. Repeated high precision EPMA analyses yielded an average Al content of 78.3 ± 5.9 ppm (1σ , $n = 41$), suggesting that Al concentrations in olivine can be measured accurately, with repeatability of 7.6 % ($1\sigma_{\text{rel}}$) at ~ 80 ppm Al. The second in-house reference material, SC/KA, does not have an 'accepted' Al concentration, but is homogenous in Ca (Köhler & Brey 1990). Repeated analyses yielded an average Al content of 89.7 ± 5.2 ppm (1σ , $n = 15$), or a repeatability of 5.8 % ($1\sigma_{\text{rel}}$) at ~ 90 ppm Al. The Al-in-olivine measurements from Winnipegosis Komatiite samples are expected to be of higher precision than this due to their higher Al contents of $\sim 250 - 450$ ppm (see Results). By comparing measured and theoretical precisions for several trace elements in the two olivine standards, we demonstrate that the repeatability of trace element measurements in olivine using the EPMA are dominated by counting statistics, at least at low concentrations (Supplementary Information). Using the formula of Cox (1983), we conservatively estimate the uncertainty on an individual measurement of Al in the Winnipegosis Komatiite olivine to be ~ 2.5 % ($1\sigma_{\text{rel}}$).

For the application of the Al-in-olivine thermometer (Coogan et al. 2014), olivine-chromite pairs were selected in which the chromite was entirely enclosed in fresh olivine, in the two dimensions observable (Figure 2a). To minimise the possible effects of secondary fluorescence from the chromite, Al-in-olivine analyses were located approximately 40 microns from the chromite grain boundaries. To account for the effects of Al zoning, 5 spots were analysed in each olivine from a range of positions around the included chromite grain. Temperatures were determined for each olivine spot using the average Cr# obtained for the enclosed chromite, and an average temperature calculated for each olivine.

5. Results

5.1 Bulk rock geochemistry

5.1.1 XRF major and minor elements

Variations of elements measured by XRF are shown in Figure 4. Some incompatible elements, such as Al_2O_3 and TiO_2 , show extremely tight correlations which extrapolate through measured olivine compositions. Others show more scatter and regression lines extend to higher (e.g. CaO) or lower (e.g. Na₂O) MgO than Winnipegosis olivine. Samples from borehole RP12 lie along the same regression trends as the RP1A samples, but are generally more scattered.

The elements SiO_2 , FeO, and MnO show less variability with MgO, but all show slightly negative correlations. Cr_2O_3 , compatible in both olivine and chromite, shows a strong positive correlation with MgO. A regression of Cr_2O_3 against MgO from RP1A intersects a mixing line between the average olivine composition and the average chromite composition at approximately 1.1 % chromite.

Samples from massive flows contain between 16.8 and 26.1 wt% MgO. Samples from the upper portion of differentiated flows generally show lower MgO contents: random olivine spinifex samples contain 15.3 – 19.8 wt% MgO, the hopper olivine cumulate sample contains 18.2 wt% MgO, and two acicular pyroxene samples both contain ~10.5 wt% MgO. Data from the GSC database indicate that most of the komatiites sampled form a tight range in MgO, with a mean of 22.2 ± 2.2 wt% ($1\sigma_{\text{absolute}}$), and a median MgO content of 22.4 wt% MgO ($n = 189$ samples with < 1 wt% CO_2).

5.1.2 ICP-MS minor and trace elements

Many trace elements measured for this study show broad negative correlations with MgO (Figure 5), though the degree of data scatter about these correlations varies considerably. In general, the heavy REEs

(HREEs) and middle REEs (MREEs) show tighter correlations with MgO, and intersect the MgO axis closer to measured olivine MgO than the light REEs (LREEs). Data for the LILEs and Pb are generally very scattered; U, Th and Nb show moderate degrees of scatter, whereas Zr, Hf, V, and Sc show tight correlations with MgO. Nickel and Co show strong positive correlations with MgO.

Primitive upper mantle (PUM) normalised spidergrams (Figure 6) show a generally depleted pattern, with $LREE < MREE$, low Nb, U and Th, and trace element concentrations approximately 2 * PUM. The samples also show a modest HREE depletion relative to the MREEs, defining 'hump' shaped REE patterns. The LILEs and Pb are variably enriched. Trace element patterns for massive flows from RP1A and RP12 are extremely consistent and there is no significant difference between boreholes. Samples from differentiated flows from RP12 show more variable patterns, and slight positive Eu anomalies are observed in two spinifex-textured samples (RP12-282.5 and RP12-305.3). Sample RP12-282.5 also shows significantly more depleted LREEs than any other sample.

5.2 Mineral Chemistry

5.2.1 Olivine

Randomly selected fresh olivine from samples RP1A-8, RP1A-18, RP1A-99, and RP1A-111 show a range of Mg# between 0.923 and 0.889 (where $Mg\# = \text{molar Mg}/[\text{Mg} + \text{Fe}]$), with a strong peak in relative frequency about 0.907 (Figure 7). To avoid Fe-enriched domains, only olivine cores were analysed; high Mg# olivine is likely over-represented. A set of 160 olivine core analyses from the GSC database, measured from 62 samples, shows an indistinguishable mode at Mg# 0.905. Olivine grains selected for Al-in-olivine thermometry are excluded from the histogram as the five points measured per olivine would bias the distribution. However, these show consistently lower Mg# than the randomly selected points, with a range in Mg# from 0.912 to 0.872, and a mode at 0.902 (150 analyses, 30 olivine grains).

The elements Ca, Mn, Al, and Co in olivine are negatively correlated with Mg#, whereas Ni and Cr show

positive correlations (Figure 8). High concentrations of Ca and Cr preclude these olivine grains from being mantle-derived xenocrysts (Simkin & Smith 1970). Some analyses from chromite-hosting olivine grains show scatter towards higher Cr contents. Modelling using the PENEPMA program (Llovet et al. 2012) shows that this is likely caused by secondary fluorescence from enclosed chromite, which can affect olivine Cr data by >100 ppm at distances up to 100 microns from the grain boundary. These analyses are not excluded from the Al-in-olivine thermometry as they do not show similarly elevated Al contents; modelling shows secondary fluorescence of Al should fall to <1 ppm levels within 15 microns of the olivine-chromite boundary. Phosphorus was below the limit of determination of 0.01 wt%, and so coupled Al-P ↔ Si-Si substitution should have a minimal effect on the calculated temperatures (Coogan et al. 2014). The consistent trends between trace elements in olivine and Mg# indicate that altered Fe-enriched domains were successfully avoided during analysis.

5.2.2 Chromite

Chromite grains measured for Al-in-olivine – spinel thermometry have Cr# ($\text{Cr\#} = \text{Cr}/[\text{Cr} + \text{Al}]$) in the range 0.64 – 0.72, overlapping the calibrated range of the thermometer (Cr# 0 – 0.69; Coogan et al. 2014). Stoichiometrically determined (Droop 1987) chromite Fe^{3+} contents (0.12 – 0.20 Fe^{3+} cations pfu) lie slightly outside the thermometer calibration range. However, the correlation between Fe^{3+} and temperature within the calibrated range is considered weak (Coogan et al. 2014) or non-existent (Wan et al. 2008), affecting calculated temperatures by less than the overall uncertainty in the calibration of ± 25 °C. We also note that the calculated Fe^{3+} contents of Winnipegosis chromite fall well within the range observed for chromite from Phanerozoic LIPs (0.07 – 0.23 Fe^{3+} cations pfu; Coogan et al. 2014), and do not show evidence of replacement by metamorphic magnetite (e.g., Evans & Frost 1975). All chromite grains analysed contain <0.5 wt% MnO, and pass the Barnes (1998) MnO vs. Mg# filter for post-eruptive alteration. Some small chromite grains yielded SiO_2 values up to several wt%, significantly larger than those typically expected for komatiitic chromites (up to 0.23 wt%; Barnes, 1998). We attribute this to secondary fluorescence from the host olivine, and use an arbitrary cut-off of 0.5 wt% SiO_2 to screen out affected analyses.

5.2.3 Al-in-olivine temperatures

Average Al-in-olivine temperatures from olivine-chromite pairs are shown in Figure 7, plotted as a function of olivine Mg#. The olivine-chromite pairs are grouped by sample and Fe-Mg exchange equilibration temperature (Ballhaus et al. 1991). Open symbols indicate Fe-Mg equilibration temperatures <900 °C, which suggest that the olivine-chromite pairs underwent extensive subsolidus exchange of Fe and Mg with their host olivines. In general, these pairs retain high, magmatic Al-in-olivine temperatures, confirming that this thermometer is less susceptible to resetting by diffusion than Mg-Fe exchange thermometers (Wan et al. 2008). However, it should be noted that the lowest Al-in-olivine temperatures at a given Mg# are from pairs with low Fe-Mg equilibration temperatures, which may indicate limited subsolidus Al exchange in some cases of extensive subsolidus Fe-Mg exchange. The Al-in-olivine temperatures range from ~1425 to ~1320 °C and correlate with Mg#. None of the chromite-hosting olivine crystals analysed had Mg# >0.912 adjacent to the chromite inclusions.

The average uncertainty ($1\sigma_{\text{abs}}$ of five Al measurements in each olivine) is ± 14 °C, less than the uncertainty in the thermometer calibration. However, these uncertainties are generally far larger than analytical errors, with the largest uncertainty of ± 33 °C ($1\sigma_{\text{abs}}$) reflecting an uncertainty in the measured Al concentration of ± 14 % ($1\sigma_{\text{rel}}$). This, combined with the relative constancy of temperatures determined from other olivine - chromite pairs (as low as ± 4 °C, $1\sigma_{\text{abs}}$) is best explained by zoning in the Al content of some olivine grains (Coogan et al. 2014).

6. Discussion

6.1 Olivine control and screening for the effects of alteration

Strong correlations between MgO and many incompatible elements that intersect olivine compositions are indicative of olivine control; consistent with the petrographical observation that olivine was the dominant crystallising mineral. A regression of Cr₂O₃ against MgO for the RP1A samples intersects a mixing line between average olivine and chromite compositions at 1.1 ± 0.1 % chromite (95 % confidence interval), suggesting the spread of data can be explained by the addition/subtraction of a mixture of ~98.9 % olivine and 1.1 % chromite phenocrysts (by weight). The proportions in this mixture must have remained relatively constant to produce such a linear trend in Cr₂O₃ against MgO, and were similar for komatiites from both the RP1A and RP12 boreholes.

Without evidence of any further phenocryst phases in the vast majority of samples, we interpret deviations from olivine (or olivine + chromite) control lines as representing alteration of primary compositions (Lahaye & Arndt 1996), for example during Trans-Hudson age metamorphism. Small deviations from olivine control lines in the differentiated flow samples may also be caused by pyroxene fractionation, but this will not affect most samples. We consider elements 'unaltered' if regressions against MgO intersect measured olivine compositions, and qualitatively identify increasing degree of alteration by:

1. Increasing scatter about regression lines (relative to the expected scatter from analytical uncertainties)
2. Increasing shift of the extrapolation of these regressions away from measured olivine compositions.

By these measures SiO₂, Al₂O₃, TiO₂, Hf, Zr, the MREEs and HREEs (Sm and heavier), Sc, and Ni are 'unaltered' in RP1A; this also implies that MgO is effectively unaltered in these rocks. Elements showing evidence of alteration, arranged in approximate order of increasing alteration are Nd < Pr < CaO ~ V < Ce < P₂O₅ < La < Th ~ Nb ~ U ~ Cu < Na₂O < Sr < K₂O ~ Ba ~ Rb ~ Cs ~ Pb (Figures 4 and 5).

The REE regressions against MgO are summarised in a 'REE alteration plot' (Figure 9). This plot is generated by plotting the R^2 value, used as a proxy for data scatter, and MgO intercept of regressions of each REE against MgO in turn. For example, a regression of Yb against MgO (Figure 5) intersects the MgO axis at 49 wt%, within the range of measured olivine compositions, and has a high R^2 value >0.9 . The Yb data therefore follow a tight olivine control line, and Yb is considered unaltered. By contrast, a regression of La against MgO extends to an MgO value of 55 wt%, higher than measured olivine compositions, and has a low R^2 value of ~ 0.55 . The La data is not consistent with an olivine control line, and La is therefore considered altered. The rapid shift towards lower R^2 values and higher MgO intercepts for LREEs lighter than Sm is indicative of increasing degrees of alteration.

We ascribe the surprisingly low degree of alteration of CaO to its incorporation primarily into dendritic clinopyroxene, which was unaltered during metamorphism. Alteration of elements in which the rock budget is dominated by chromite (Cr_2O_3), or which may be strongly affected by changing olivine partition coefficients (FeO, MnO, Ni) cannot be checked by this method, but the low degrees of scatter about regressions against MgO suggest Cr_2O_3 , FeO, MnO, and Ni are also close to unaltered in RP1A samples.

6.2 Metamorphism vs. mixing of depleted and enriched components

Samples from borehole RP12, metamorphosed at greenschist facies, show far greater scatter in plots of fluid-mobile elements such as Na_2O , Sr, K_2O , Ba, Rb, Cs, and Pb against MgO than the lower grade RP1A samples (prehnite-pumpellyite facies). This seems to indicate that metamorphism is the primary cause of deviations from olivine control lines. However, this fails to explain the scatter in elements such as Nb, U, and Th, given that data for these elements from samples in the higher metamorphic grade RP12 borehole show a tighter correlation with MgO than the less metamorphosed RP1A samples (e.g. Figure 5). Significant mobility during metamorphism would be especially surprising for Nb given that all other high field strength elements and even 'more mobile' elements such as Ca show tight correlations against MgO, and Nb is not

typically mobile during low grade metamorphism (Cann 1970).

In an attempt to resolve this issue, we test the possibility that both the flat trace element patterns of Winnipegosis Komatiites and the high degree of scatter of generally fluid immobile elements such as Nb and Th could reflect variable mixing between a depleted komatiite magma and more enriched component: enriched mantle in the source, subduction-zone fluids, or continental crust.

We model the depleted komatiite magma using the DMORB estimate of Gale et al. (2013) normalised to Lu in the Winnipegosis samples, and plot mixing trends between this melt and various enriched components in Figure 10. The effect of an enriched component in the mantle source is modelled as a vector towards EMORB (Gale et al. 2013); subduction zone fluids are modelled as vectors towards high Sr (shallow subduction component) and Th (deep subduction component) at constant Nb/Yb (Pearce & Stern 2006); and contamination by local continental crust is modelled as mixing with Superior Craton tonalites from borehole RP92-5. The observation that Sr, Th and Nb are significantly elevated relative to depleted MORB (Figure 10a) rules out subduction zone fluids as the enriching component, as these should increase non-conservative elements such as Sr and Th without significantly increasing Nb (Pearce & Stern 2006). Although on a Th/Yb vs Nb/Yb plot (Figure 10b) the Winnipegosis samples lie on the boundary of the MORB-OIB array of Pearce (2008), there is no purely 'oceanic' (i.e., mantle derived) component that can cause such large and variable enrichments in both Th and Nb, and still plot within the MORB-OIB array. We therefore interpret slight enrichments in Th relative to Nb compared to DMORB as being caused by continental crustal contamination. Figure 10c shows that mixing the Lu-normalised DMORB composition with 1 – 3 % Superior craton tonalite results in a trace element pattern that closely approximates those of Winnipegosis Komatiite samples.

6.2.1 Effect of crustal contamination

Even for a mixture containing 3% assimilated continental crust, less than 10% of the total budget of

elements more compatible than Hf would be supplied from assimilated continental crust, hence variable amounts of assimilation of these elements at any stage of the magmatic system should have a negligible effect on olivine control lines. By contrast, 21 – 45 % of Nb in the final, assimilated melt would arise from the small amount (1 – 3 % respectively) of assimilated continental crust. As such, even small variations in the amount of continental crust assimilated as magmatism progressed could cause significant variations in the final Nb content of the magma, leading to the observed scatter in regressions of Nb vs MgO. This interpretation is supported by the observation that samples from different parts of the lava pile in RP1A lie on different trends of Nb vs. MgO (Figure 5). The increase in Nb content up-section is consistent with an increasing Nb contribution from crustal contaminants as magmatism progressed.

In summary, a small but variable amount of crustal contamination can explain both the scatter about olivine control lines observed for strongly incompatible but fluid immobile elements such as Nb and Th, and the flat trace element patterns of Winnipegosis samples. A combination of crustal contamination and mobility during metamorphism may be invoked to explain the large scatter in strongly incompatible fluid mobile elements such as Ba, Rb, Cs, and Pb.

6.3 Winnipegosis samples are Proterozoic komatiites

6.3.1 Olivine-liquid Fe-Mg exchange

We use olivine-liquid Fe-Mg exchange to ascertain the parental liquid MgO content of the Winnipegosis Komatiites (e.g. Nisbet et al. 1993). To use this method, an appropriate exchange coefficient must be selected (exchange coefficient, $K_{D,Fe^{2+}-Mg}^{ol-liq} = (FeO/MgO)^{ol}/(FeO/MgO)^{liq}$, hereafter K_D), and the approximate $Fe^{2+}/\sum Fe$ of the magmas must be known. As K_D varies with liquid MgO (Herzberg & Hara 2002), we choose an olivine K_D of 0.345, determined for bulk compositions similar to those of the Winnipegosis (Matzen et al. 2011).

Determining the appropriate $Fe^{2+}/\sum Fe$ is more challenging, and we use three independent methods to arrive at an estimate (see Supplementary Information for details). Firstly, the $Fe^{2+}/\sum Fe$ of liquids in equilibrium with chromite can be calculated from the chromite Fe^{2+}/Fe^{3+} ratio (Maurel & Maurel 1982; Larsen & Pedersen 2000). The Ballhaus et al. (1991) olivine-spinel Fe-Mg exchange thermometer was used to screen out chromite grains which had undergone extensive subsolidus re-equilibration with their host olivines, as indicated by low olivine-spinel Fe-Mg exchange temperatures. The Fe-Mg exchange temperature was found to negatively correlate with chromite Fe^{2+}/Fe^{3+} ratios, implying some chromite grains had gained Fe^{2+} during subsolidus exchange. The least altered chromite indicates a liquid $Fe^{2+}/\sum Fe$ of 0.90 at identical Fe-Mg and Al-in-olivine temperatures of 1398 ± 27 °C and 1391 ± 9 °C respectively. Secondly, V/Sc partitioning (Lee et al. 2005), indicates an $Fe^{2+}/\sum Fe$ of ~ 0.95 for melting predominantly in the spinel stability field (of the upper mantle), and ~ 0.98 for melting predominantly in the garnet stability field. Finally, we note that the best fit of olivine Fe-Mg partitioning to Al-in-olivine temperatures (Figure 7 and section 6.4) appears to be for $Fe^{2+}/\sum Fe \approx 0.9$, though the 'resolution' of this comparison is poor due to uncertainties in the Al-in-olivine temperatures.

Our preferred value of $Fe^{2+}/\sum Fe$ is 0.90, calculated from chromite compositions, as this provides the best constrained estimate of $Fe^{2+}/\sum Fe$ at the time of komatiite crystallisation, and is identical to previous estimates of komatiite $Fe^{2+}/\sum Fe$ (Berry et al. 2008). This may represent a lower bound on the $Fe^{2+}/\sum Fe$ at the liquidus if olivine crystallisation consumed Fe^{2+} in the melt before chromite began to crystallise (Section 6.4). By contrast, V/Sc partitioning calculates the average fO_2 at the point the komatiites separated from their source, and provides an upper bound due to the likelihood that Winnipegosis Komatiites assimilated continental crust (Section 6.2).

6.3.2 Parental liquid MgO

Using $K_D = 0.345$ and $Fe^{2+}/\sum Fe = 0.90$, the highest Mg# olivine (0.923) crystallised from a liquid containing 23.6 wt% MgO and 11.3 wt% FeO . The largest uncertainties on this parental melt composition

arise from the $Fe^{2+}/\sum Fe$ ratio of the melt and uncertainties in the maximum Mg# measured in olivine. If the higher $Fe^{2+}/\sum Fe$ values calculated from V/Sc partitioning are used, the parental melt MgO is elevated to 24.8 wt% for melting in the spinel field, and 25.6 wt% for melting in the garnet field, though these are likely to represent upper bounds (Section 6.3.1). An uncertainty of ± 0.005 in the maximum Mg# of 0.923 results in calculated MgO ranging from 22.1 to 25.2 wt%; because this error is dominated by systematic differences between analytical sessions (Supplementary Information), it cannot be reduced by multiple measurements of the same olivine. However, we believe the parental liquid MgO to be more robust than indicated by this, as we measured 6 olivine grains with Mg# > 0.92 (out of a total of 183 randomly selected olivines), and 9 olivine grains in the GSC database have Mg# > 0.92 (n = 160 olivine cores). The similar proportion of olivine analyses with Mg# > 0.92 measured in different labs robustly indicates the presence of olivines with Mg# > 0.92.

The calculated parental liquid MgO of 23.6 wt%, which lies well within the range of Winnipegosis bulk rock compositions, confirms that these rocks are komatiites (Arndt & Brooks 1980). The presence of olivine spinifex in at least three flows in borehole RP12 means the Winnipegosis rocks also satisfy the definition of komatiite of Kerr & Arndt (2001). Supporting this interpretation is the fact that the median MgO, over a large number of samples covering two ~250 m thick sections of lava is 22.4 wt% MgO, with an average estimated olivine phenocryst content of 17 vol%; these samples certainly do not represent small volume eruptions of a highly olivine-charged picrite. Finally, the composition of chill margins from the GSC database show a range of MgO between 19.6 wt% and 23.4 wt% (17 chill samples with < 1 wt% CO₂). Correcting for petrographically-estimated olivine phenocryst contents of 5 – 20 vol %, the residual liquids at the time of eruption were komatiite or basaltic komatiite, with olivine-corrected MgO approximately in the range 14.1 – 20.3 wt%.

6.4 Thermal evolution of Winnipegosis Komatiite melts

6.4.1 Liquidus Temperature

We use the relationship of Matzen et al. (2011) to equate the parental melt MgO content of 23.6 wt% MgO to a liquidus temperature of 1501 ± 32 °C for the Winnipegosis Komatiite parental melt (2σ uncertainty calculated allowing ± 0.005 uncertainty in olivine Mg#). Use of the Primelt3 software (Herzberg & Asimow 2015) corroborates this high liquidus temperature independent of measured olivine compositions. A liquidus temperature of 1492 ± 20 °C at a parental melt MgO of 23.2 ± 0.7 wt% (2σ of all bulk rock compositions that did not experience clinopyroxene fractionation) is calculated for batch melting. Calculations assuming accumulated fractional crystallisation failed as the Winnipegosis compositions are too low in CaO to have been produced by fractional melting of fertile peridotite.

This liquidus temperature is ~ 100 °C lower than upper-end estimates of the liquidus temperatures of Archaean komatiites (Nisbet et al. 1993; Robin-Popieul et al. 2012; Sossi & O'Neill 2016). However, it is not significantly higher than temperatures suggested for some Phanerozoic magmas, such as unerupted komatiitic magmas from the Etendeka LIP (Thompson & Gibson 2000), and the West Greenland picrites (Larsen & Pedersen 2000).

This calculation of the liquidus temperature can be more generally extended to a relationship between Mg# of olivine and temperature (Supplementary Information):

$$T = \frac{19.2 * b}{\frac{m_{FeO}}{K_D * m_{MgO}} \left(\frac{1}{Mg\#} - 1 \right) - a} + 1048$$

where a and b are the gradient and intercept of a linear regression of bulk rock FeO vs. MgO ($FeO = a * MgO + b$) at a given $Fe^{2+} / \sum Fe$, m_{FeO} and m_{MgO} are the molar masses of FeO and MgO respectively.

Temperature – Mg# curves for our preferred value of $Fe^{2+}/\sum Fe = 0.90$, as well as values calculated from Fe-Mg exchange are shown in Figure 7. Use of the MgO-dependent K_D parameterisation of Herzberg & Hara (2002) leads to 7 – 13 °C higher temperatures, but almost parallel curves (not shown) due to a weak variation of K_D at high liquid MgO contents. Allowing for scatter of data and possible systematic errors, the Al-in-olivine temperatures are an excellent match to those predicted by anhydrous olivine Fe-Mg partitioning for $Fe^{2+}/\sum Fe \sim 0.90$, confirming the high liquidus temperatures calculated above.

6.4.2 Hydrous komatiites?

Recently, Sobolev et al. (2016) revived the idea that some Archaean komatiites may originate from a hydrous transition zone source (Kawamoto et al. 1996). For comparison, Figure 7 also shows a curve for $Fe^{2+}/\sum Fe = 0.90$, with a ~60 °C depression of the liquidus predicted for 0.5 wt% H₂O (Falloon & Danyushevsky 2000). This predicts temperatures that are too low to be consistent with the majority of Al-in-olivine temperatures. As the Al-in-olivine thermometer is not influenced by magmatic H₂O content or fO_2 (Coogan et al. 2014), this suggests the Winnipegosis magmas are nominally anhydrous, and did not arise from a hydrous source. This interpretation is supported by the MORB-like trace element patterns and low Ce content of the komatiites, which predict ~0.04 – 0.1 wt% H₂O in the parental melt for H₂O/Ce of 100 – 250 respectively (Dixon et al. 2002).

6.4.3 Cooling and crystallisation history

Using the comparison between the Al-in-olivine thermometer and olivine Fe-Mg partitioning, we can reconstruct the cooling history of the Winnipegosis magmas (Figure 11). Liquidus olivine crystallised from a melt containing 23.6 wt% MgO at a temperature of 1501 ± 32 °C. Olivine was the sole crystallising phase over an interval between 1501 °C and ~1424 °C, the highest Al-in-olivine temperature recorded by coexisting olivine and chromite in all three samples studied. The spread in temperature of the first olivine-chromite pairs to crystallise from each sample is small, but absolute uncertainties of ± 25 °C arising from the

calibration of the Al-in-olivine thermometer are likely to be larger than this spread, so we infer that the olivine-chromite cotectic was reached at 1424 ± 25 °C, from a liquid MgO of 19.6 ± 1.3 wt%. If the first crystallisation of chromite is calculated instead from the highest average Mg# measured for olivine enclosing chromite (Mg# = 91.1), an indistinguishable (within uncertainty) temperature of 1440 ± 24 °C, or liquid MgO of 20.4 ± 1.3 wt% is obtained.

Olivine and chromite continued to crystallise until at least 1321 ± 25 °C (14.2 ± 1.3 wt% MgO, calculated from Al-in-olivine temperature), or 1328 ± 13 °C (14.6 ± 0.7 wt% MgO, calculated from Fe-Mg partitioning) in RP1A-99, the least MgO rich sample for which Al-in-olivine temperatures were obtained. However, we find no evidence of such low temperatures in RP1A-8 and RP1A-111, both of which had higher bulk rock MgO. This liquid MgO content, from which the lowest temperature olivine and chromite pair crystallised, is similar to the lowest MgO estimated for a chill margin after olivine phenocryst subtraction (~ 14.1 wt%). Thus, 1321 ± 25 °C may provide an approximation to the lowest temperature at which Winnipegosis Komatiites erupted. After eruption the growth of olivine phenocrysts effectively ceased, and olivine crystallisation continued only as skeletal overgrowths on existing phenocrysts, and crystallisation of hopper and dendritic olivine in the groundmass. From the observation that pyroxene dendrites are always interstitial to olivine dendrites, and by analogy to the experiments of Faure & Tissandier (2014), we infer that pyroxene crystallisation did not commence until the temperature had fallen considerably and olivine dendrite growth had ceased.

6.5 Bulk rock compositions are not liquid compositions – the role of mixing

The inference that chromite did not begin to crystallise until liquid MgO content reached <21.7 wt% has profound implications for the understanding of bulk rock geochemical trends. If the bulk rock compositions are interpreted as a liquid line of descent (LLD), then Cr_2O_3 would be expected to increase with falling MgO until ~ 20 wt% MgO was reached, before falling once chromite began to crystallise. Instead, Cr_2O_3 is positively correlated with MgO for all samples. This positive correlation, and by extension all other olivine

control lines, is best understood as a mixing line between a residual melt and a phenocryst mixture of olivine and chromite. Due to the largely constant volume proportion of phenocrysts throughout each flow, this mixing likely occurred before or during magma eruption. Solid-liquid mixing can also explain why plots of FeO, MnO, and Ni against MgO are closely approximated by straight lines (Figures 4, 5), whereas the LLD for each of these elements should be curved as the crystallising olivine becomes progressively rich in FeO and MnO, and depleted in Ni. Mixing is also evidenced by the wide range of olivine compositions in each sample, which do not correlate with bulk rock MgO (Supplementary Information).

We model the liquid line of descent (LLD) for the Winnipegosis Komatiites through incremental addition and subtraction of olivine (Albarede 1992; Larsen & Pedersen 2000) from a parental melt composition defined by the intersection of bulk-rock element regressions against MgO with 23.6 wt% MgO (Figure 12). At each step, the composition of olivine in equilibrium with the melt is calculated (assuming fixed $Fe^{2+} / \sum Fe = 0.90$ and constant K_d of 0.345), and added or removed from the melt composition; this corresponds to fractional crystallisation. For simplicity, olivine was assumed to contain only SiO_2 , MgO and FeO, and chromite was ignored due to its volumetrically small contribution and uncertainty in the ratio of olivine to chromite crystallising at a given temperature.

For incompatible elements such as Al_2O_3 , LLDs are indistinguishable from the observed mixing lines, as their relationships with MgO are insensitive to the exact Mg# of olivine being added or subtracted (Francis 1985). However, as the FeO/MgO ratio of an olivine depends on the FeO/MgO ratio of the liquid from which it crystallised, the predicted LLD in FeO vs. MgO space deviates more strongly from the observed bulk rock compositions. Despite this, the FeO predicted for the LLD never varies from the regression of bulk rock compositions by >0.4 wt% FeO over the range of bulk rock MgO observed in the Winnipegosis Komatiites (10 – 26 wt% MgO). This has a smaller effect on parental melt compositions and liquidus temperatures than the range of $Fe^{2+} / \sum Fe$ calculated or the uncertainty in the Mg# of the most magnesian olivine. The largest deviation from the LLD will occur in Cr_2O_3 vs MgO due to the extremely strong dependence of bulk rock Cr_2O_3 on volumetrically small addition or subtraction of chromite.

6.6 Aluminium-undepleted Winnipegosis Komatiites

Winnipegosis Komatiites have slightly sub-chondritic $\text{Al}_2\text{O}_3/\text{TiO}_2$ (17.2 ± 0.2 , $1\sigma_{\text{abs}}$), and slightly supra-chondritic Gd/Yb (Figure 13), placing them between average Al-depleted ($\text{Al}_2\text{O}_3/\text{TiO}_2 \sim 11$) and Al-undepleted komatiite ($\text{Al}_2\text{O}_3/\text{TiO}_2 \sim 20$; Nesbitt et al. 1979). Olivine-corrected molar $[\text{Al}_2\text{O}_3]$ and $[\text{TiO}_2]$ values of 0.191 and 0.0142, respectively, identifies them as Al-undepleted komatiites according to the classification of Hanski et al. (2001). In terms of trace element patterns (Figure 6), Winnipegosis Komatiites are quite similar to other Al-undepleted komatiites (e.g. Alexo, Lahaye & Arndt 1996) showing a generally incompatible element-depleted trend. Their slight HREE depletion relative to the MREEs is somewhat unusual for an Al-undepleted komatiite, but parallels the slight HREE depletion observed in Gorgona 'G1' komatiites (Revillon et al. 2000). Contents of ~ 46.3 wt% SiO_2 calculated for the parental melt at 23.6 wt% MgO place the Winnipegosis komatiites in the low SiO_2 group of Parman & Grove (2005), similar to Munro komatiites and with a distinctly lower SiO_2 at a given MgO than Barberton komatiites.

7. Tectonic Interpretation

7.1 Winnipegosis Komatiite Belt as part of the Circum-Superior Belt

The new 1870.3 ± 7.1 Ma age of the Winnipegosis Komatiite Belt is identical, within uncertainty, to the youngest mafic and ultramafic bodies previously dated in the Circum-Superior Belt, both in the adjacent Thompson Nickel Belt and more than 2000 km away in the New Quebec Orogen (Heaman et al. 2009). The Winnipegosis Komatiites also share many petrological features with other igneous rocks of the CSB: mafic/ultramafic rocks are abundant; magmatic olivine with $Mg\# \geq 0.92$, indicative of high temperature melts, has been reported from other regions of the CSB (Arndt et al. 1987); and depleted, MORB-like compositions are widespread (Heaman et al. 2009). Therefore, the tectonic interpretation of the Winnipegosis Komatiites cannot take place in isolation, and should be considered as a segment of the wider CSB.

7.2 Formation model

A model for the formation of the Winnipegosis Komatiites must satisfy the following geochemical evidence outlined in this study: 1) formation of high MgO, high liquidus temperature parental magmas with no evidence of significant depression of the liquidus due to the presence of water; 2) low absolute trace element abundances, approximately twice that of primitive mantle; 3) generally depleted trace element signatures indicating a DMORB-like source; 4) evidence of crustal contamination.

We also consider the following geological and geochronological evidence to be important: 5) the unconformable relationship of the WKB over Superior craton tonalites; 6) the transition from tholeiitic basalt to komatiite up-section within the WKB; 7) the transition in sedimentation style from a short interval of conglomerates and sandstones at the base of the WKB to carbonates and shales at higher stratigraphic levels (Burnham et al. 2009; McGregor 2011); 8) formation in a convergent margin setting (Section 2; Corrigan et al. 2009; Heaman et al. 2009); 9) age identical, within uncertainty, to both pericratonic arc

magmatism in the Snow Lake Arc (Percival et al. 2005), and mafic – ultramafic magmatism in the Circum-Superior Belt (Heaman et al. 2009).

7.2.1 Emplacement of Winnipegosis Komatiites over rifted Superior Craton crust

As the Winnipegosis Komatiites were sourced from mantle similar to the DMORB source, high degrees of melting – combined with little crystal fractionation before eruption – are required to explain the low concentrations of incompatible elements. This is consistent with the high calculated liquidus temperatures. However, the Winnipegosis Komatiites were emplaced upon continental crust (points 4 and 5 above), as previously recognised for many Archaean komatiites and greenstone belts (Bickle et al. 1994; Pearce 2008). This observation rules out oceanic settings where high degrees of melting are observed such as mid-ocean ridges, and plume-generated oceanic plateaux. Instead, we propose that the high degrees of melting necessary to produce the Winnipegosis Komatiites are best explained by their emplacement within an evolving rift, near the Superior Craton margin. A rift setting is also consistent with points 6 and 7; the progression of volcanism from tholeiitic basalt to komatiite up section could represent increasing mantle melting as rifting progressed, and the style of sedimentation is consistent with a rift environment.

7.2.2 Thermal anomaly or ambient mantle?

Whether or not the Winnipegosis Komatiites can be generated from ambient mantle or require thermally anomalous mantle depends critically on the potential temperature of the mantle during the Palaeoproterozoic. Traditional models of secular mantle cooling (e.g. Davies 1999) suggest that Palaeoproterozoic mantle potential temperatures (T_p) may not have been significantly higher than today, with $T_p \approx 1300$ °C at 1.9 Ga relative to a modern MORB $T_p = 1220$ °C ($\Delta T \approx 80$ °C). In this case a thermal anomaly is clearly required to produce Winnipegosis magmas with a liquidus temperature of 1501 °C. By contrast, Herzberg et al. (2010) argue that the Proterozoic ambient mantle was capable of producing primary melts with MgO of 18 – 24 wt%, with ambient T_p as high as 1600 °C at ~1.9 Ga (relative to a modern

MORB T_p of 1350 ± 50 °C, $\Delta T \approx 250$ °C). However, *all* of the highest temperature estimates ($T_p > 1500$ °C) for Proterozoic magmas examined by Herzberg et al. (2010) are for samples from the Cape Smith Belt, part of the larger Circum-Superior Belt. As the Circum-Superior Belt has previously been interpreted as a plume-derived LIP (Ernst & Bleeker 2010; Minifie et al. 2013), the evidence for high T_p estimates in ambient Proterozoic mantle is equivocal.

Excluding samples from the Cape Smith Belt, the highest T_p suggested for the Proterozoic by Herzberg et al. (2010) is ~ 1490 °C for the 2056 Ma Lapland basalts. Given the inevitable temperature drops due to the latent heat of fusion and decompression during ascent, ambient mantle of $T_p = 1490$ °C cannot produce the Winnipegosis Komatiites. Calculations using Primelt3 software (Herzberg & Asimow 2015) indicate mantle T_p of 1644 ± 33 (2σ of all bulk rock compositions that did not experience clinopyroxene fractionation) for Winnipegosis compositions. As such, the formation of the Winnipegosis Komatiites likely requires thermally anomalous mantle, regardless of the model of mantle thermal history used. This is supported by the observation that the MgO content of the Winnipegosis Komatiites is substantially higher than the average MgO content of mafic rocks during the Palaeoproterozoic, which was similar to the present day at <10 wt% MgO (Keller & Schoene 2012).

7.2.3 A model for the Winnipegosis Komatiites and Circum-Superior Belt

The requirement of above ambient mantle temperatures to generate the Winnipegosis Komatiites allows us to rule out several models previously suggested for the Circum-Superior Belt, which generate high degrees of melting but do not predict elevated mantle temperatures (Heaman et al. 2009 and references therein). Instead, we believe the formation of the WKB and the wider CSB are best explained as a mantle plume derived LIP (Ernst & Bleeker 2010; Minifie et al. 2013).

In addition to generating above ambient mantle temperatures and high degrees of melting, a plume origin is consistent with the relatively short time span (1885 – 1870 Ma) of the majority of CSB magmatism (Heaman et al. 2009). Within the WKB, erosion of the underlying Superior Craton tonalites can also be

understood as occurring during a period of plume-driven uplift, followed by extensive volcanism and deposition of sediments occurring as rifting continued.

However, a number of other features of the CSB require refinement of a simple plume model. Despite the relatively tight age range for the majority of CSB mafic/ultramafic magmatism, the revised age of 1870.3 ± 7.1 Ma for the WKB extends the range of mean ages for ~ 1.9 Ga CSB magmatism to ~ 30 Myrs, with no evidence for a progressive migration of the magmatism over time (Heaman et al. 2009). The distribution of magmatism along ~ 3000 km of continental margin also appears at odds with the expectation of approximately equant plume heads (Campbell & Griffiths 1990).

We suggest that these inconsistencies can be resolved by a 'focussed' plume model (Figure 14), in which an upwelling plume is deflected to the margins of the Superior Craton by the underlying thick cratonic lithosphere (Thompson & Gibson 1991; Sleep et al. 2002; Minifie et al. 2013), and interacts with a series of pre-existing rifts around the Superior margin. The presence of pre-existing rifts in the CSB, either due to back arc rifting or pull apart basins formed by oblique convergence (Skulski & Wares 1993), might be expected due to convergence and closure of the Manikewan Ocean along the northern and western margins of the Superior Craton (Section 2; Corrigan et al. 2009). This is especially clear for the WKB, which formed contemporaneously with, and inboard of, the pericratonic Snow Lake Arc (Percival et al. 2005), and therefore plausibly formed over lithosphere thinned in a back arc setting.

The presence of rifts around the Superior margin would have generated a steep lithospheric gradient between the centre of the craton and its margins, focussing the plume head and leading to the observed distribution of magmatism around the craton margins. This type of lithospheric control on the distribution of komatiitic magmatism has previously been suggested for Archaean komatiites of the Yilgarn craton (Mole et al. 2014). Pre-existing rifts can also explain the large, ~ 30 Myr spread in magmatic ages. In our model, magmatism in back arc or pull apart rifts accounts for the earliest ~ 1900 Ma magmatism (Heaman et al. 2009), with the arrival of a plume causing a large outpouring of high temperature magmatism at $1885 -$

1870 Ma. Our model differs from previous plume models for the CSB in that we envisage the plume impinging beneath the Superior craton and emphasise the control of lithospheric architecture in deflecting plume material towards the craton margins, rather than impinging outboard of the northern margin of the Superior craton (Ernst & Bleeker 2010). Decompression and therefore melting would have been limited beneath the thick Superior Craton lithosphere, though plume impingement may have triggered the generation of numerous carbonatite complexes in the Superior Craton at ~ 1.88 Ga (Rukhlov & Bell 2010).

8. Conclusions

The Winnipegosis Komatiites formed at 1870.3 ± 7.1 Ma as part of the Circum-Superior Belt LIP. They occur as both massive and differentiated flows containing olivine spinifex layers. Their parental melt contained ~ 24 wt% MgO, which, along with the presence of spinifex layers and a median MgO of 22.4 wt% over >250 m thickness of flows, confirms that these lavas are Proterozoic komatiites.

The parental melts crystallised only olivine from 1501 °C to approximately 1424 °C, and then a mixture of olivine + chromite phenocrysts until eruption at approximately 1321 °C. Olivine and chromite phenocrysts were entrained and variably mixed with residual melts shortly before and/or during eruption. Bulk rock compositions represent mixing lines between these phenocryst phases rather than the liquid line of descent.

The coincidence of Al-in-olivine temperatures with temperatures calculated from olivine Fe-Mg partitioning requires that the mantle source of the Winnipegosis Komatiites was nominally dry. This is supported by trace element patterns, which indicate a DMORB like, dry, parental melt. This melt was subsequently contaminated by small amounts of assimilated Superior craton continental crust, through which the Winnipegosis magmas erupted. Low absolute abundances of trace elements are consistent with high calculated liquidus temperatures, indicating high degrees of mantle melting. In the context of the broader Circum-Superior Belt, we suggest the Winnipegosis Komatiites were generated by a mantle plume that was deflected towards the margins of the Superior craton by strong gradients in lithospheric thickness. The interpretation of the Circum-Superior Belt as a plume derived LIP casts doubt on ambient mantle potential temperatures as high as 1600 °C during the Proterozoic (Herzberg et al. 2010).

Acknowledgements

Pedro Waterton performed this work under the tenure of an NSERC Vanier Scholarship at the University of Alberta. Analytical work was funded by the Canada Excellence Research Chairs Program and the Geological Survey of Canada. We thank Stan Mertzman and Karen Mertzman for the XRF analyses, and Thomas Stachel and Gerhard Brey for supplying and discussing olivine standards. Constructive discussions with Yannick Bussweiler, Richard Stern, Tom Chacko, Mark Hamilton, Richard Ernst and Larry Heaman were a great help during the preparation of this work. We also thank Philippe Pagé and Laurence Coogan for constructive reviews, and Andrew Kerr for editorial handling. B.M. Saumur is thanked for internal GSC review.

References

- Albarede, F., 1992. How deep do common basaltic magmas form and differentiate? *Journal of Geophysical Research*, 97(B7), p.10997.
- Ansdell, K.M. et al., 1995. Kiseynew metasedimentary gneiss belt, Trans-Hudson orogen (Canada): back-arc origin and collisional inversion. *Geology*, 23(11), pp.1039–1043.
- Ansdell, K.M., 2005. Tectonic evolution of the Manitoba-Saskatchewan segment of the Paleoproterozoic Trans-Hudson Orogen, Canada. *Canadian Journal of Earth Sciences*, 42(4), pp.741–759.
- Arndt, N. & Brooks, C., 1980. Komatiites. *Geology*, 8, pp.155–156.
- Arndt, N., Leshner, C.M. & Barnes, S.J., 2008. *Komatiite*, Cambridge: Cambridge University Press.
- Arndt, N.T. et al., 1987. Geochemistry, petrogenesis and tectonic environment of Circum- Superior Belt basalts, Canada. Geological Society Special Publications No. 33. In *Geochemistry and Mineralization of Proterozoic Volcanic Suites*. Blackwell Scientific Publications, pp. 133–145.
- Arndt, N.T., 1982. Proterozoic spinifex-textured basalts of Gilmour Island, Hudson Bay. In *Current Research, Part A, Geological Survey of Canada, Paper 82-1A*. Geological Survey of Canada, pp. 137–142.
- Arndt, N.T. & Leshner, C.M., 1992. Fractionation of REEs by olivine and the origin of Kambalda komatiites, Western Australia. *Geochimica et Cosmochimica Acta*, 56(12), pp.4191–4204.
- Baldwin, D.A. et al., 1987. U-Pb zircon ages from the Lynn Lake and Rusty Lake metavolcanic belts, Manitoba: two ages of Proterozoic magmatism. *Canadian Journal of Earth Sciences*, 24(5), pp.1053–1063.
- Ballhaus, C., Berry, R.F. & Green, D.H., 1991. High pressure experimental calibration of the olivine-orthopyroxene-spinel oxygen geobarometer: implications for the oxidation state of the upper mantle. *Contributions to Mineralogy and Petrology*, 107(1), pp.27–40.
- Baragar, W.R.A. & Scoates, R.F.J., 1981. The Circum-Superior Belt: A Proterozoic plate margin? In A. Kroner, ed. *Developments in Precambrian Geology*. pp. 297–330.

- Barnes, S.J., 1998. Chromite in Komatiites , 1. Magmatic Controls on Crystallization and Composition. *Journal of Petrology*, 39(10), pp.1689–1720.
- Barnes, S.J. & Often, M., 1990. Ti-rich komatiites from northern Norway. *Contributions to Mineralogy and Petrology*, 105(1), pp.42–54.
- Berry, A.J. et al., 2008. Oxidation state of iron in komatiitic melt inclusions indicates hot Archaean mantle. *Nature*, 455(7215), pp.960–963.
- Bickle, M.J. et al., 1976. Mantle composition derived from the chemistry of ultramafic lavas. *Nature*, 263, pp.577–580.
- Bickle, M.J., Nisbet, E.G. & Martin, a., 1994. Archean Greenstone Belts Are Not Oceanic Crust. *The Journal of Geology*, 102(2), pp.121–137.
- Burnham, O.M. et al., 2009. *CAMIRO Project 97E-02, Thompson Nickel Belt: final report March 2002, revised and updated 2003*,
- Campbell, I.H. & Griffiths, R.W., 2014. Did the formation of DPrime; cause the Archaean-Proterozoic transition? *Earth and Planetary Science Letters*, 388, pp.1–8.
- Cann, J.R., 1970. Rb, Sr, Y, Zr and Nb in some ocean floor basaltic rocks. *Earth and Planetary Science Letters*, 10(1), pp.7–11.
- Coogan, L.A., Saunders, A.D. & Wilson, R.N., 2014. Aluminum-in-olivine thermometry of primitive basalts: Evidence of an anomalously hot mantle source for large igneous provinces. *Chemical Geology*, 368(0), pp.1–10.
- Corrigan, D., 2012. Paleoproterozoic crustal evolution and tectonic process: Insights from the Lithoprobe program in the Trans Hudson Orogen, Canada. In J. A. Percival, F. A. Cook, & R. M. Clowes, eds. *Special Paper 49. Tectonic styles in Canada: The Lithoprobe perspective*. Geological Association of Canada, pp. 237–284.
- Corrigan, D. et al., 2009. The Palaeoproterozoic Trans-Hudson Orogen: a prototype of modern accretionary processes. In J. B. Murphy, J. D. Keppie, & A. J. Hynes, eds. *Geological Society, London, Special*

Publications. Special Publications. Geological Society, London, pp. 457–479.

Cox, M.G., 1983. Experimental Determination of X-ray Intensities. In V. D. Scott & G. Love, eds. *Quantitative Electron-Probe Microanalysis*. Chichester: Ellis Horwood Limited, pp. 125–146.

David, J., Bailes, A.H. & Machado, N., 1996. Evolution of the Snow Lake portion of the Palaeoproterozoic Flin Flon and Kiseynew belts, Trans-Hudson Orogen, Manitoba, Canada. *Precambrian Research*, 80(1–2), pp.107–124.

Davies, G.F., 1999. *Plates, Plumes and Mantle Convection*, Cambridge: Cambridge University Press.

Dixon, J.E. et al., 2002. Recycled dehydrated lithosphere observed in plume-influenced mid-ocean-ridge basalt. *Nature*, 420(6914), pp.385–389.

Droop, G.T.R., 1987. A general equation for estimating Fe³⁺ concentrations in ferromagnesian silicates and oxides from microprobe analyses, using stoichiometric criteria. *Mineralogical Magazine*, 51, pp.431–435.

Echeverria, L.M., 1980. Tertiary or Mesozoic komatiites from Gorgona Island, Colombia: Field relations and geochemistry. *Contributions to Mineralogy and Petrology*, 73(3), pp.253–266.

Ernst, R. & Bleeker, W., 2010. Large igneous provinces (LIPs), giant dyke swarms, and mantle plumes: significance for breakup events within Canada and adjacent regions from 2.5 Ga to the Present. *Canadian Journal of Earth Sciences*, 47(5), pp.695–739.

Evans, B.W. & Frost, B.R., 1975. Chrome-Spinel in Progressive Metamorphism - Preliminary Analysis. *Geochimica et Cosmochimica Acta*, 39(6–7), pp.959–972.

Falloon, T.J. & Danyushevsky, L. V, 2000. Melting of Refractory Mantle at 1.5, 2 and 2.5 GPa under Anhydrous and H₂O-undersaturated Conditions: Implications for the Petrogenesis of High-Ca Boninites and the Influence of Subduction Components on Mantle Melting. *J. Petrol.*, 41(2), pp.257–283.

Faure, F. & Tissandier, L., 2014. Contrasted Liquid Lines of Descent Revealed by Olivine-hosted Melt Inclusions and the External Magma. *Journal of Petrology*, 9(0), pp.1779–1798.

Francis, D., 1985. The Baffin Bay lavas and the value of picrites as analogues of primary magmas.

Contributions to Mineralogy and Petrology, 89(2–3), pp.144–154.

Gale, A. et al., 2013. The mean composition of ocean ridge basalts. *Geochemistry, Geophysics, Geosystems*, 14(3), pp.489–518.

Hanski, E. et al., 2004. Origin of the Permian-Triassic komatiites, northwestern Vietnam. *Contributions to Mineralogy and Petrology*, 147(4), pp.453–469.

Hanski, E. et al., 2001. The Palaeoproterozoic Komatiite – Picrite Association of Finnish Lapland. *Journal of Petrology*, 42(5), pp.855–876.

Heaman, L.M., Peck, D. & Toope, K., 2009. Timing and geochemistry of 1.88 Ga Molson Igneous Events, Manitoba: Insights into the formation of a craton-scale magmatic and metallogenic province. *Precambrian Research*, 172(1–2), pp.143–162.

Herzberg, C., Condie, K. & Korenaga, J., 2010. Thermal history of the Earth and its petrological expression. *Earth and Planetary Science Letters*, 292(1–2), pp.79–88.

Herzberg, C. & Hara, M.J.O., 2002. Plume-Associated Ultramafic Magmas of Phanerozoic Age. *Journal of Petrology*, 43(10), pp.1857–1883.

Herzberg, C.T. & Asimow, P.D., 2015. PRIMELT3 MEGA.XLSM software for primarymagma calculation: Peridotite primarymagma MgO contents from the liquidus to the solidus. *Geochemistry, Geophysics, Geosystems*, 16, pp.563–578.

Hofmann, A.W., 1988. Chemical differentiation of the Earth: the relationship between mantle, continental crust, and oceanic crust. *Earth and Planetary Science Letters*, 90(3), pp.297–314.

Hollings, P. & Ansdell, K., 2002. Paleoproterozoic arc magmatism imposed on an older backarc basin: Implications for the tectonic evolution of the Trans-Hudson orogen, Canada. *GSA Bulletin*, 114(2), pp.153–168.

Hulbert, L. et al., 1994. The Winnipegosis komatiite belt, central Manitoba. In *Manitoba Mining and Minerals Convention 1994, Program and Abstracts*. p. 21.

- Hulbert, L.J. et al., 2005. U-Pb zircon and Re-Os isotope geochronology of mineralized ultramafic intrusions and associated nickel ores from the Thompson Nickel Belt, Manitoba, Canada. *Economic Geology*, 100(1), pp.29–41.
- Hynes, A. & Francis, D.M., 1982. A transect of the early Proterozoic Cape Smith foldbelt, New Quebec. *Tectonophysics*, 88, pp.23–59.
- IAG, 2015. IAG Certified Reference Materials. Available at: <http://www.iageo.com/index.php/certified-reference-materials.html>.
- JCGM, 2008. JCGM 200 : 2008 International vocabulary of metrology — Basic and general concepts and associated terms (VIM) Vocabulaire international de métrologie — Concepts fondamentaux et généraux et termes associés (VIM). *International Organization for Standardization Geneva ISBN*, 3(Vim), p.104.
- Jolly, W.T., 1982. Progressive metamorphism of komatiites and related Archaean lavas of the abitibi area, Canada. In N. T. Arndt & E. G. Nisbet, eds. *Komatiites*. London: George Allen & Unwin, pp. 247–266.
- Kawamoto, T., Hervig, R.L. & Holloway, J.R., 1996. Experimental evidence for a hydrous transition zone in the early Earth's mantle. *Earth and Planetary Science Letters*, 142(3–4), pp.587–592.
- Keller, C.B. & Schoene, B., 2012. Statistical geochemistry reveals disruption in secular lithospheric evolution about 2.5 Gyr ago. *Nature*, 485(7399), pp.490–493.
- Kerr, A.C. & Arndt, N.T., 2001. A Note on the IUGS Reclassification of the High-Mg and Picritic Volcanic Rocks. *Journal of Petrology*, 42(11), pp.2169–2171.
- Köhler, T. & Brey, G., 1990. Calcium exchange between olivine and clinopyroxene calibrated as a geothermobarometer for natural peridotites from 2 to 60 kb with applications. *Geochimica et Cosmochimica Acta*, 54(9), pp.2375–2388.
- Lahaye, Y. & Arndt, N.T., 1996. Alteration of a Komatiite Flow from Alexo, Ontario, Canada. *Journal of Petrology*, 37(6), pp.1261–1284.
- Larsen, L.M. & Pedersen, A.K., 2000. Processes in High-Mg, High-T Magmas: Evidence from Olivine,

Chromite and Glass in Palaeogene Picrites from West Greenland. *Journal of Petrology*, 41(7), pp.1071–1098.

Lee, C.-T.A. et al., 2005. Similar V/Sc Systematics in MORB and Arc Basalts: Implications for the Oxygen Fugacities of their Mantle Source Regions. *Journal of Petrology*, 46(11), pp.2313–2336.

Llovet, X. et al., 2012. Secondary fluorescence in electron probe microanalysis of material couples. *Journal of Physics D: Applied Physics*, 45(22), p.225301.

Lucas, S.B. et al., 1993. Deep seismic profile across a Proterozoic collision zone: surprises at depth. *Nature*, 363, pp.339–342.

Machado, N., Zwanzig, H. & Parent, M., 1999. U-Pb ages of plutonism, sedimentation, and metamorphism of the Paleoproterozoic Kiseynew metasedimentary belt, Trans-Hudson Orogen (Manitoba, Canada). *Canadian Journal of Earth Sciences*, 36(11), pp.1829–1842.

Maier, W.D. et al., 2009. Progressive mixing of meteoritic veneer into the early Earth's deep mantle. *Nature*, 460(7255), pp.620–623.

Matzen, A.K. et al., 2011. Fe-Mg Partitioning between Olivine and High-magnesian Melts and the Nature of Hawaiian Parental Liquids. *Journal of Petrology*, 52(7–8), pp.1243–1263.

Maurel, C. & Maurel, P., 1982. Etude expérimentale de l'équilibre Fe^{2+} - Fe^{3+} dans les spinelles chromifères et les liquides silicatés basiques coexistants 1 atm. *Comptes Rendus de l'Académie des Sciences*, 295, pp.209–212.

McGregor, C.R., 2011. *Open File OF2011-1: GIS compilation of relogged sub-Phanerozoic Precambrian exploration drillcore from the Thompson Nickel Belt, eastern Flin Flon Belt and Winnipegosis Komatiite Belt (parts of NTS 63B, C, F, G, J, K)*,

Mertzman, S., 2000. K-Ar results from the southern Oregon-northern California Cascade Range. *Oregon Geology*, 62(4), pp.99–122.

Minifie, M.J. et al., 2013. The northern and southern sections of the western ca. 1880 Ma Circum-Superior Large Igneous Province, North America: The Pickle Crow dyke connection? *Lithos*, 174(0), pp.217–235.

- Nesbitt, R.W., Sun, S.-S. & Purvis, A.C., 1979. Komatiites: geochemistry and genesis. *Canadian mineralogist*, 17, pp.165–186.
- Nisbet, E.G. et al., 1993. Constraining the potential temperature of the Archaean mantle: A review of the evidence from komatiites. *Lithos*, 30(3–4), pp.291–307.
- Ottley, C.J., Pearson, D.G. & Irvine, G.J., 2003. A routine method for the dissolution of geological samples for the analysis of REE and trace elements via ICP-MS. In J. G. Holland & S. D. Tanner, eds. *Plasma Source Mass Spectrometry: Applications and Emerging Technologies*. Cambridge: The Royal Society of Chemistry, pp. 221–230.
- Pagé, P. & Barnes, S.-J., 2009. Using Trace Elements in Chromites to Constrain the Origin of Podiform Chromitites in the Thetford Mines Ophiolite, Québec, Canada. *Economic Geology*, 104(7), p.997 LP-1018.
- Parman, S.W. et al., 1997. Emplacement conditions of komatiite magmas from the 3.49 Ga Komati Formation, Barberton Greenstone Belt, South Africa. *Earth and Planetary Science Letters*, 150, pp.303–323.
- Parman, S.W. & Grove, T.L., 2005. Komatiites in the Plume Debate. *Geological Society Of America Special Papers*, 388, pp.249–256.
- Pearce, J.A., 2008. Geochemical fingerprinting of oceanic basalts with applications to ophiolite classification and the search for Archean oceanic crust. *Lithos*, 100(1–4), pp.14–48.
- Pearce, J.A. & Stern, R.J., 2006. Origin of Back-Arc Basin Magmas : Trace Element and Isotope Perspectives. In *Geophysical Monograph Series, Volume 166. Back-Arc Spreading Systems: Geological, Biological, Chemical, and Physical Interactions*. American Geophysical Union, pp. 63–86.
- Percival, J.A., Whalen, J.B. & Rayner, N., 2005. Pikwitonei-Snow Lake Manitoba transect (parts of NTS 63J, 63O and 63P), Trans-Hudson Orogen-Superior Margin Metalotect Project: new results and tectonic interpretation. In *Report of Activities 2005, Manitoba Industry, Economic Development and Mines*. Manitoba Geological Survey, pp. 69–91.

- Potts, P.J., 1992. *A Handbook of Silicate Rock Analysis*, Springer.
- Puchtel, I.S. et al., 1997. Petrology and geochemistry of crustally contaminated komatiitic basalts from the Vetreny Belt, southeastern Baltic Shield: Evidence for an early Proterozoic mantle plume beneath rifted Archean continental lithosphere. *Geochimica et Cosmochimica Acta*, 61(6), pp.1205–1222.
- Revillon, S. et al., 2000. Geochemical Study of Ultramafic Volcanic and Plutonic Rocks from Gorgona Island, Colombia: the Plumbing System of an Oceanic Plateau. *Journal of Petrology*, 41(7), pp.1127–1153.
- Robin-Popieul, C.C.M. et al., 2012. A new model for Barberton komatiites: Deep critical melting with high melt retention. *Journal of Petrology*, 53(11), pp.2191–2229.
- Rukhlov, A.S. & Bell, K., 2010. Geochronology of carbonatites from the Canadian and Baltic shields, and the Canadian Cordillera: Clues to mantle evolution. *Mineralogy and Petrology*, 98(1–2), pp.11–54.
- Simkin, T. & Smith, J.V., 1970. Minor-element distribution in olivine. *The Journal of Geology*, 78(3), pp.304–325.
- Sobolev, A. V et al., 2016. Komatiites reveal a hydrous Archaean deep-mantle reservoir. *Nature*, 531(7596), pp.628–632.
- Sossi, P.A. & O'Neill, H.S.C., 2016. Liquidus temperatures of komatiites and the effect of cooling rate on element partitioning between olivine and komatiitic melt. *Contributions to Mineralogy and Petrology*, 171(5), p.49.
- Stauffer, M.R., 1984. Manikewan: An Early Proterozoic Ocean in Central Canada, its Igneous History and Orogenic Closure. *Precambrian Research*, 25, pp.257–281.
- Sun, S.-s. & McDonough, W.F., 1989. Chemical and isotopic systematics of oceanic basalts: implications for mantle composition and processes. *Geological Society, London, Special Publications*, 42(1), pp.313–345.
- Thompson, R.N. & Gibson, S.A., 2000. Transient high temperatures in mantle plume heads inferred from magnesian olivines in Phanerozoic picrites. *Nature*, 407, pp.502–506.

Wan, Z., Coogan, L. a. & Canil, D., 2008. Experimental calibration of aluminum partitioning between olivine and spinel as a geothermometer. *American Mineralogist*, 93(7), pp.1142–1147.

Whalen, J.B. et al., 2002. A mainly crustal origin for tonalitic granitoid rocks, Superior Province, Canada: Implications for late archean tectonomagmatic processes. *Journal of Petrology*, 43(8), pp.1551–1570.

White, D.J. et al., 2002. Suture-zone geometry along an irregular Paleoproterozoic margin: The Superior Boundary Zone, Manitoba, Canada. *Geology*, 30(8), pp.735–738.

Figure Captions

Figure 1. a) Map showing location of Winnipegosis Komatiite Belt in relation to the Circum-Superior Belt and Trans-Hudson Orogeny, modified from Baragar & Scoates (1981) and Corrigan (2012). Boundaries of cratons and CSB shown are surface exposures except Sask craton and WKB, which are have little and no surface outcrop respectively, and are identified geophysically. b) Map of the Superior Boundary Zone on the Western Superior Craton, modified from McGregor (2011) and Corrigan (2012). The portion of the map south of the thick dashed line lies beneath Palaeozoic cover: burial depth increases to southwest. Units in this region are interpreted based on aeromagnetic signatures supplemented with borehole data; 1.90 – 1.86 Ga arc plutons are only identified where aeromagnetic signatures match those in outcropping parts of Flin Flon – Snow Lake Belt (McGregor 2011). c) Reconstructed stratigraphy of the WKB based on core logging.

Figure 2: Photomicrographs of Winnipegosis komatiite in plane polarised light, with olivine (ol), chromite (chr), clinopyroxene (cpx) and glass (gl) labelled. a) Example of a chromite (in thick dashed circle) included in fresh olivine used for Al-in-olivine thermometry. b) Typical sample from near the base of a massive flow. Subhedral olivine phenocrysts with pseudomorphed skeletal overgrowths set in a matrix of clinopyroxene dendrites (typically <200 μm wide) and devitrified glass (brown). c) Typical chill margin sample: olivine phenocrysts in a matrix of straight pseudomorphed olivine dendrites, which divide patches of extremely fine grained clinopyroxene dendrites and spherulites (brown, with elongate crystals just visible). d) Random olivine spinifex layer: pseudomorphosed olivine dendrites (longest, straight crystals) divide patches of coarse clinopyroxene dendrites (shorter interstitial grains) and devitrified glass (brown), virtually phenocryst free. Note larger scale.

Figure 3: X-ray map of relative Fe content. Bright green and red equant grains are chromite with magnetite-rich metamorphic overgrowths. Olivine fragments show low Fe (blue colours) in their cores, zoning to high Fe (yellow) adjacent to serpentinised cracks.

Figure 4: Variation of major and minor elements as a function of MgO. All plots show linear regressions of RP1A data (solid black lines), along with 95% confidence limits about the regression (dashed grey curves). Cr₂O₃ vs. MgO plot shows a mixing line between the average olivine and chromite compositions, ticks indicate percentage of chromite in mixture. FeO is plotted as $0.90 * FeO_t$, based on our estimate of the $Fe^{2+} / \sum Fe$ at the time komatiite crystallisation (see Section 6.3.1. for details); plot also shows model olivine compositions as a thick black line, tick marks indicate olivine Mg#. Thin grey line represents the FeO/MgO ratio of the liquid in equilibrium with the highest Mg# olivine, and the dashed red line indicates the calculated parental liquid MgO.

Figure 5: Variation of trace elements as a function of MgO, showing linear regressions of all RP1A data with 95% confidence limits. RP1A data for Nb is split into samples from the lowermost 50 m of the borehole ('RP1A lower', orange circles) and samples from the remainder of the borehole ('RP1A upper', blue diamonds). An average value of 5.8 ppm Sc measured from LA-ICP-MS analyses of Winnipegosis Komatiite olivine (P. Waterton, unpublished data) is plotted at the average olivine MgO of 49 wt%. Scandium in chromite was not measured; although previous work has indicated up to 16 ppm Sc in chromite from high MgO volcanic rocks (Pagé & Barnes 2009), this is not expected to have a large effect on the whole rock budget of Sc due to the low proportion of chromite. Nickel in olivine and chromite were measured by EPMA. All other trace elements plotted were present in negligible quantities in Winnipegosis olivine, and assumed to be negligible in chromite; their MgO ranges are plotted at 0 ppm trace element concentration.

Figure 6: Trace element spidergram normalised to PUM (Hofmann 1988). Element order after Sun & McDonough (1989), except the position of Pb. All massive flow samples (n = 27) analysed are shown in the top diagram, samples from differentiated flows are subdivided in the lower plot. Fluid mobile elements are highlighted in grey. Thick black line is the average DMORB of Gale et al. (2013). Slight negative Zr anomalies are likely an analytical artefact (Section 4.2).

Figure 7: Average Al-in-olivine temperatures for olivine-chromite pairs, plotted as a function of olivine Mg#. Olivine-chromite pairs are grouped by sample and Fe-Mg equilibration temperature (Ballhaus et al. 1991); solid symbols indicate high equilibration temperatures (>900 °C), open symbols indicate low equilibration temperatures (<900 °C). Error bars are 1 standard deviation of the 5 repeated analyses for each olivine. Histogram (light blue blocks) and probability density function (red line) show Mg# of olivine cores (n = 183). Grey curves are temperatures determined from anhydrous olivine Fe-Mg partitioning as a function of Mg#, shown for liquid $Fe^{2+} / \sum Fe = 0.90$ (our preferred value), 0.95, and 0.98 (upper bounds determined from V/Sc partitioning). Green dotted curve shows temperature – Mg# relationship for $Fe^{2+} / \sum Fe = 0.90$ in a melt containing 0.5 wt% H₂O. See section 6.4 for details.

Figure 8: Minor and trace elements in olivine plotted as a function of Mg#. Solid black line in Cr plot is a regression of the random olivine data, with dashed lines showing 3 σ uncertainty about the regression. Only three of the random olivine data plot outside these bounds, whereas many of the analyses from olivine–chromite pairs show elevated Cr, indicative of secondary fluorescence. No similar distinction can be made for the Al data, except for the lower Mg# of the olivine–chromite pairs. Dotted lines are approximate trends for all other minor and trace elements.

Figure 9: ‘REE alteration plot’ summarising olivine control line regressions for the REEs. Thick solid blue line plots the MgO intercept of regressions of REEs data. Grey box shows range of olivine compositions measured in Winnipegosis Komatiites; to satisfy an olivine control line, the MgO intercept of REE regressions should lay within this range. Thin dashed red line shows R² value of regressions against MgO, used here as a proxy for data scatter. MREEs and HREEs have consistently high R² values of >0.9 and intersect measured olivine compositions, indicating they were unaltered. By contrast, R² values fall rapidly, and MgO intercepts are shifted to higher values than measured olivine compositions, for LREEs lighter than Sm.

Figure 10: Models of contamination of a DMORB like melt with subduction zone fluids, enriched mantle

sources, and continental crust. Tonalite data (green symbols and lines) from the GSC database (Supplementary Data); as Th was not measured for these samples, the median Th/Yb from Superior tonalites (Whalen et al. 2002) was used. a) Sr/Yb vs Nb/Yb plot modified from Pearce & Stern (2006); Sr shows far less scatter due to mobility during metamorphism than Ba. Only RP1A samples are shown as metamorphism has variably enriched Sr in most RP12 samples. b) Th/Yb vs Nb/Yb plot (Pearce 2008). Crosses and percentages indicate amount of contaminant in mixture. c) DMORB (Gale et al. 2013) normalised trace element patterns. Dotted blue line is the trace element pattern for RP1A-87, a sample with MgO content close to the calculated parental melt (Section 6.3). Solid black line is DMORB of Gale et al. (2013) normalised to Lu in RP1A-87. Grey lines show mixtures of DMORB-like melt mixed with 1, 2, and 3% tonalite.

Figure 11: Schematic cooling history of the Winnipegosis Komatiites, showing crystallising assemblage at different temperatures. Temperatures of significant events are arranged assuming monotonic cooling of a single batch of magma. Straight lines are not intended to indicate linear cooling, as we have no constraints on the cooling rate, but the break in slope separates slow cooling during phenocryst growth from rapid cooling and growth of dendritic forms after eruption. All temperatures and errors are derived from Fe-Mg partitioning for consistency.

Figure 12: Comparison of regressions of bulk rock compositions to calculated LLDs. Bulk rock data omitted for clarity, see Figure 4. Crosses are 10 wt% increments of olivine removed from parental magma by fractional crystallisation, negative percentages correspond to olivine addition. Tick marks indicate Mg# of olivine. Red tie lines link highest and lowest Mg# olivines with their respective equilibrium liquids; these are tangential to the LLD.

Figure 13: Chondrite normalised Gd/Yb ratios $(Gd/Yb)_N$ plotted as a function of Al_2O_3/TiO_2 . Winnipegosis Komatiites are compared to Al-depleted, Al-undepleted, and Al-enriched komatiites from Barberton (Robin-Popieul et al. 2012), a global database of fresh MORB (www.earthchem.org/petdb; accessed Dec. 2012),

and the primitive mantle values of Hofmann (1988). MORB are likely shifted towards lower $\text{Al}_2\text{O}_3/\text{TiO}_2$ due to plagioclase fractionation, but $(\text{Gd}/\text{Yb})_N$ should remain representative of their parental melts.

Figure 14: Schematic diagram illustrating a possible environment of formation for the Winnipegosis Komatiites. Thermally anomalous mantle generated by a mantle plume is deflected towards the margins of the Superior craton by a strong lithospheric gradient between the thick lithosphere of the Superior craton and back arc rifting along its margins.

Fig. 1

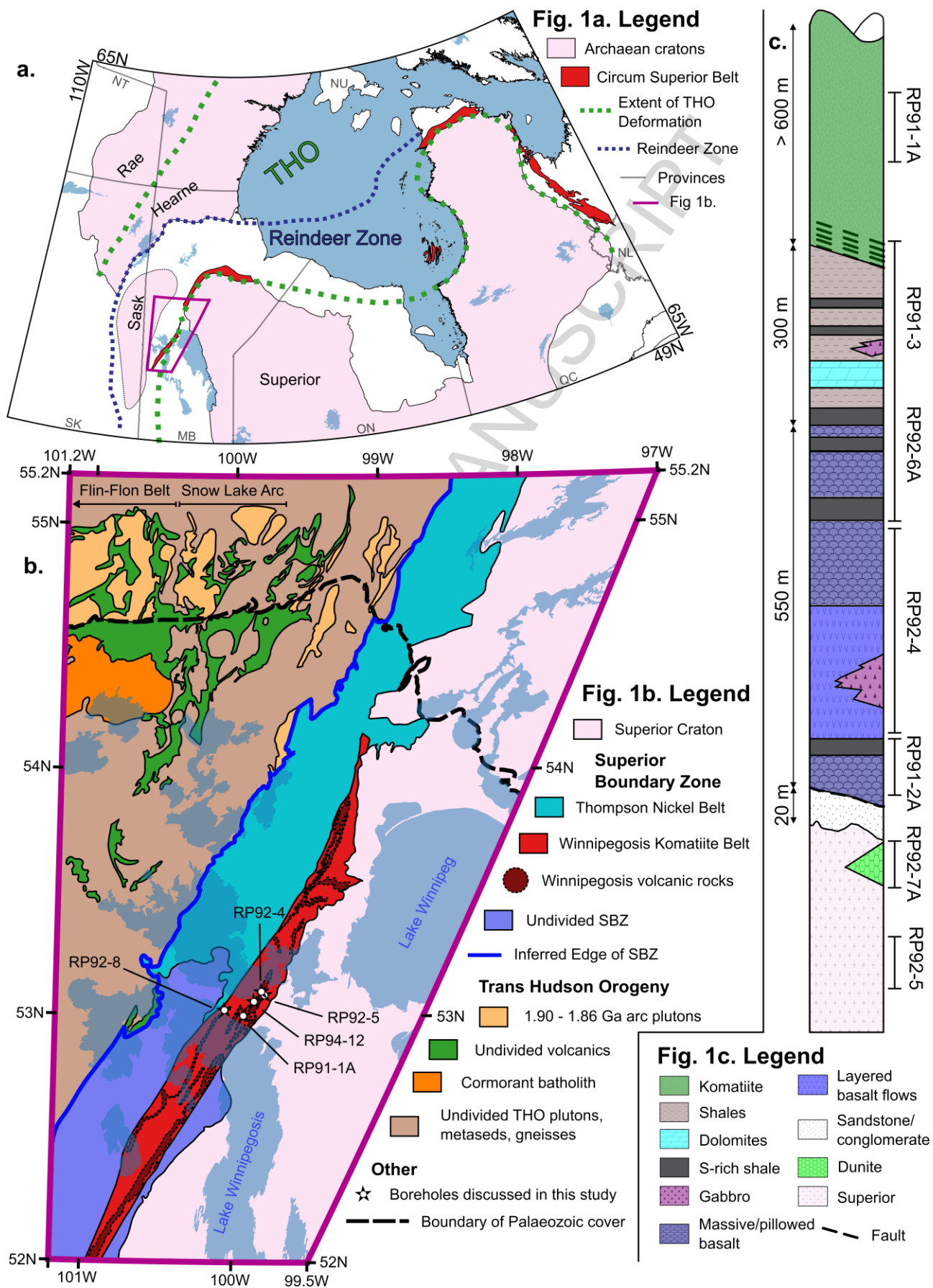


Fig. 2

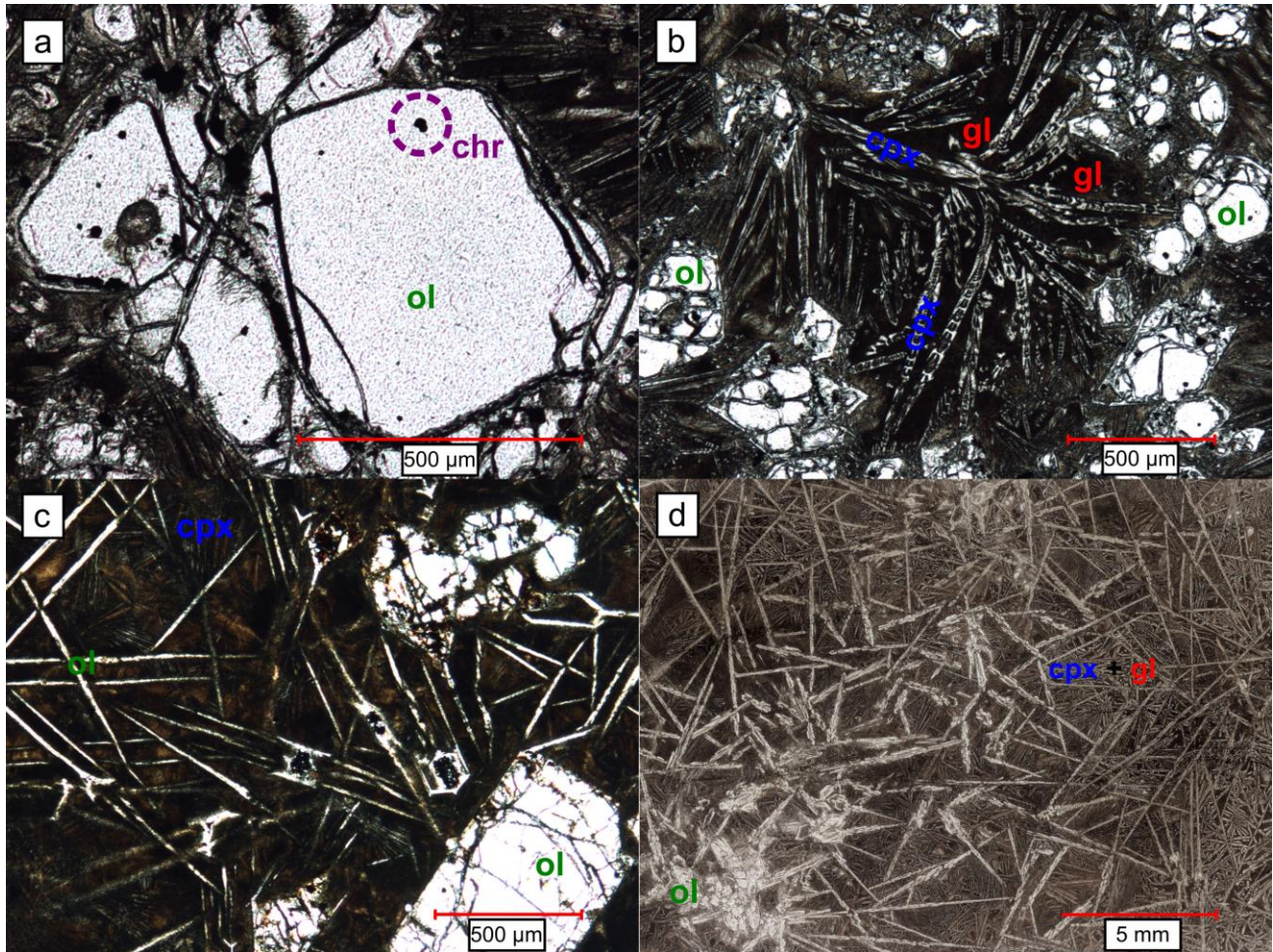


Fig. 3

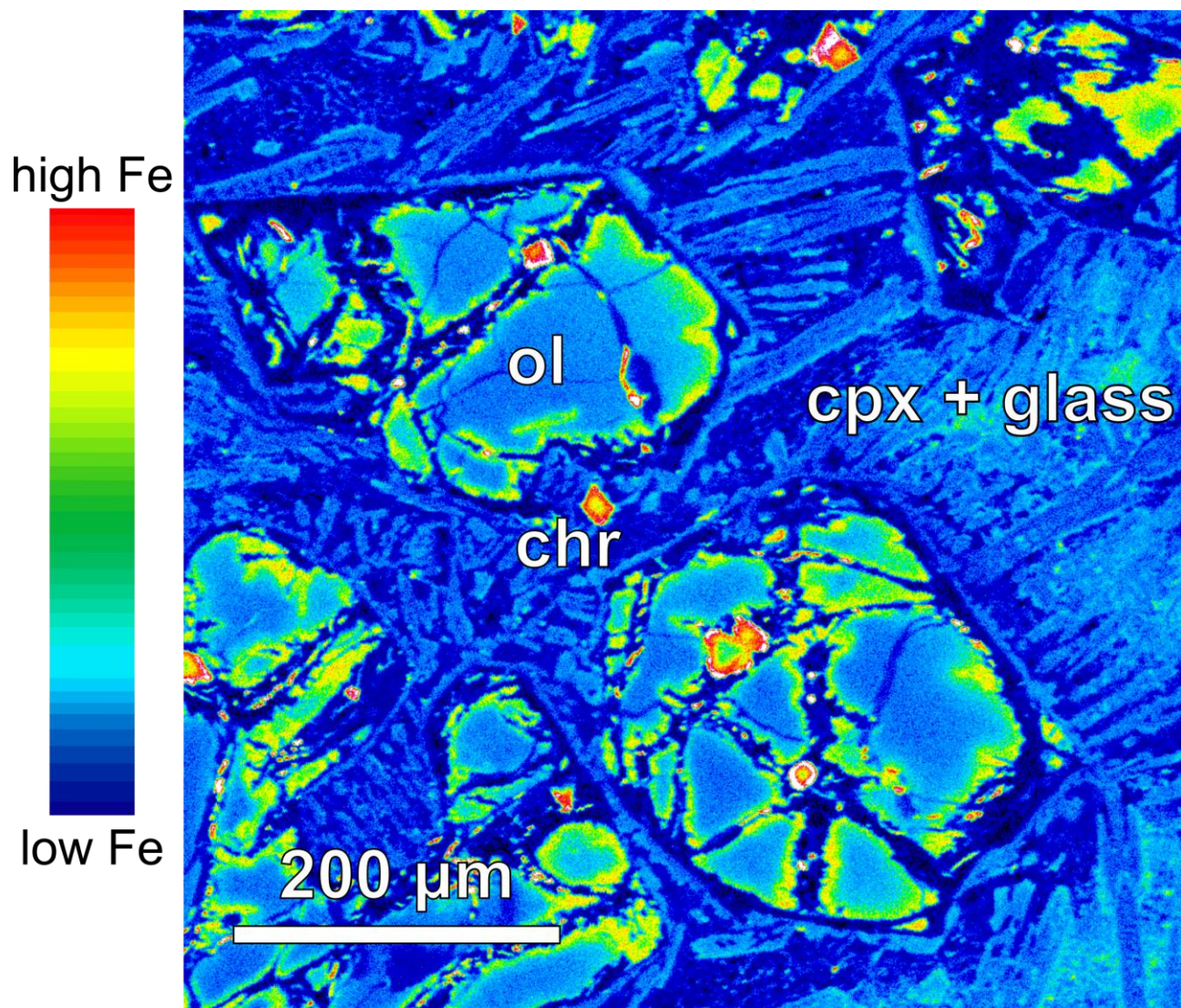


Fig. 4

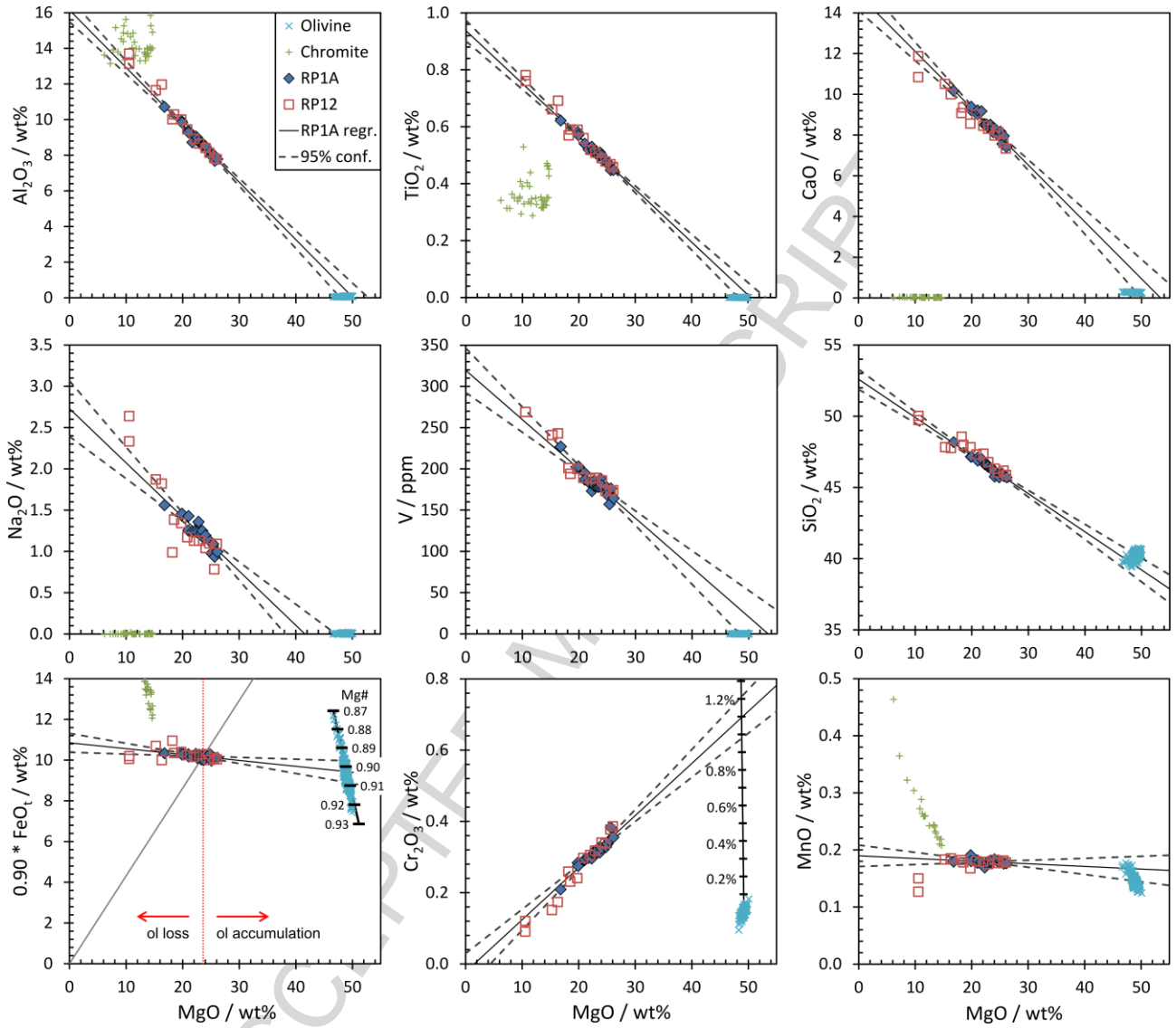


Fig. 5

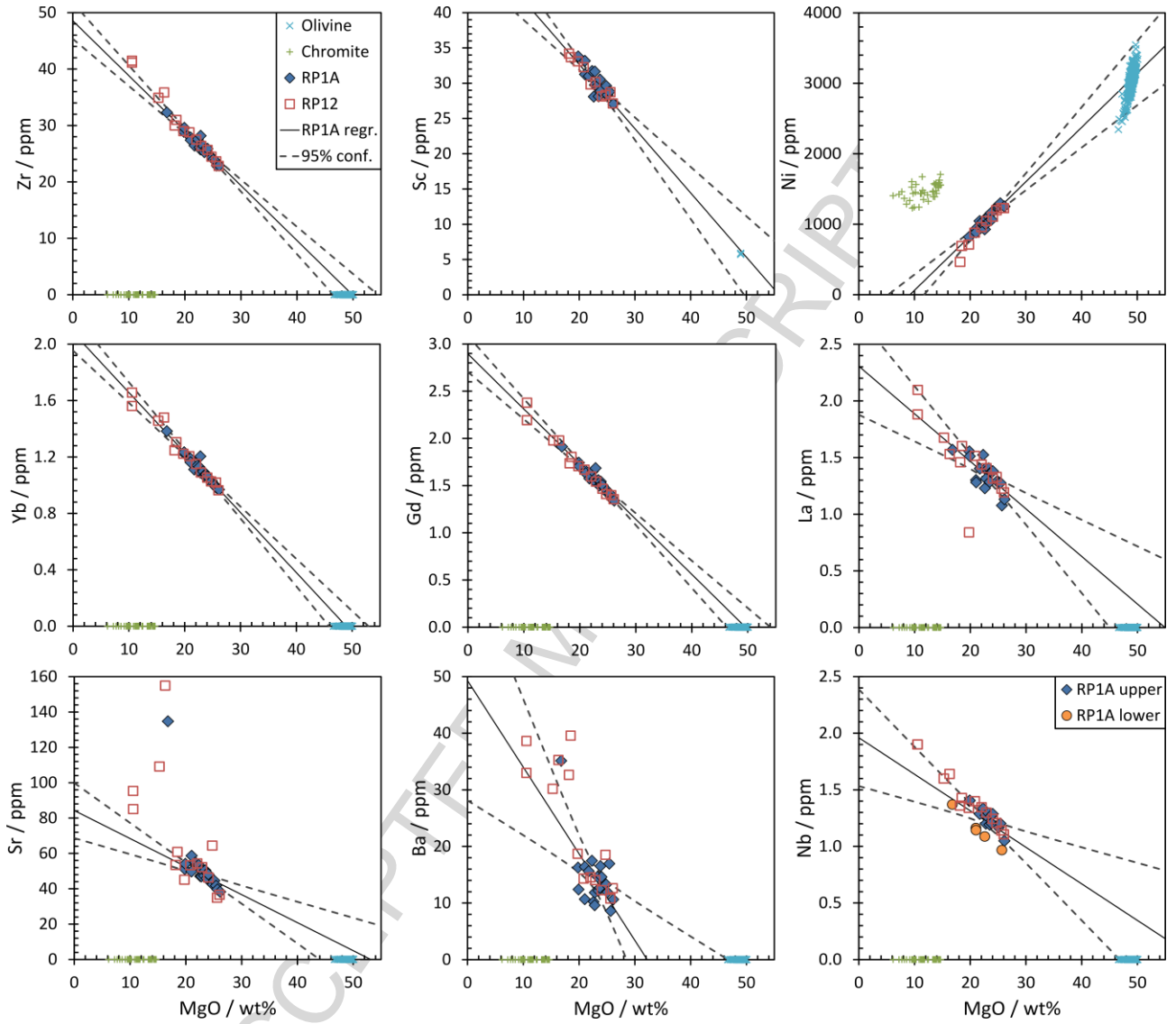


Fig. 6

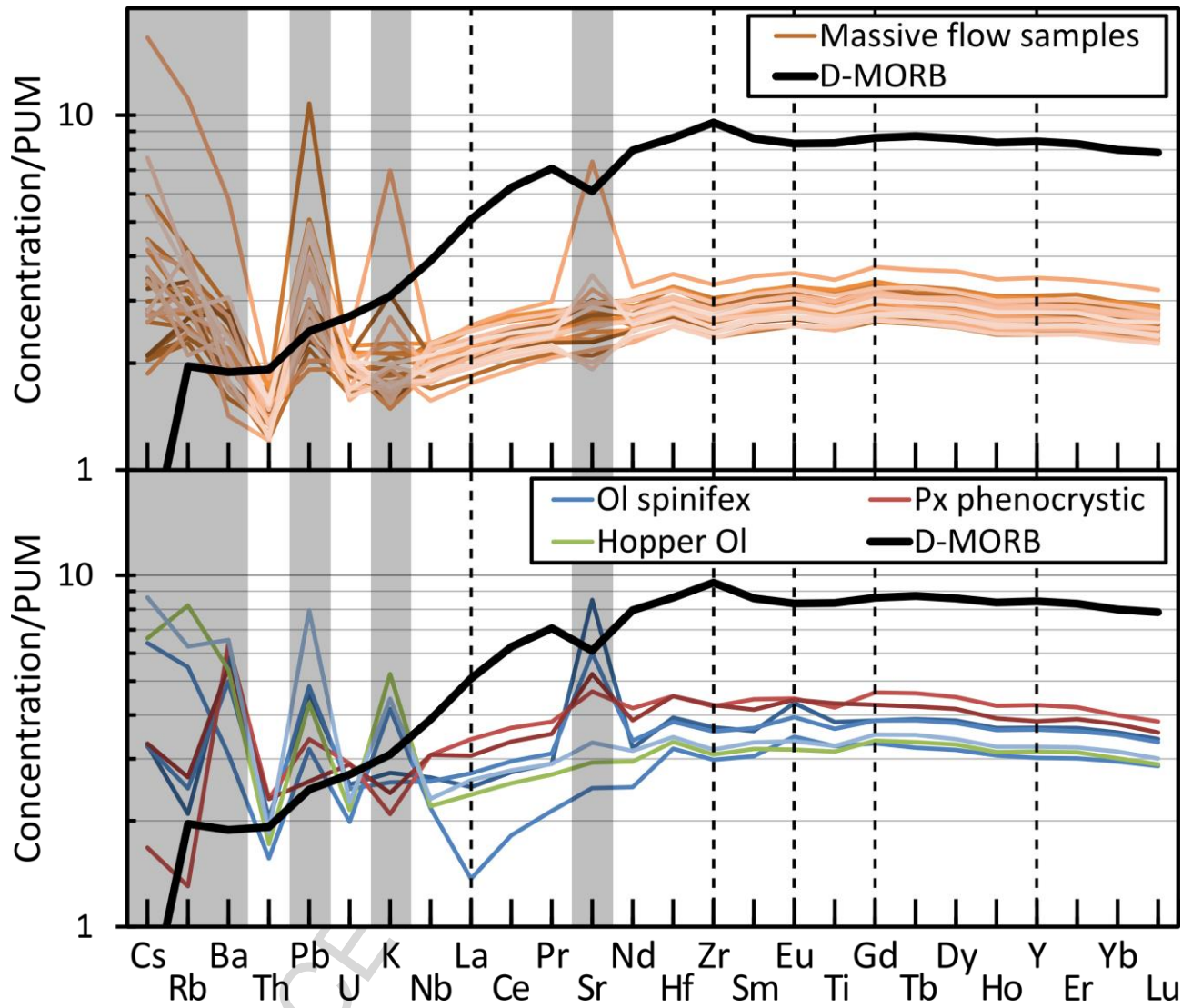


Fig. 7

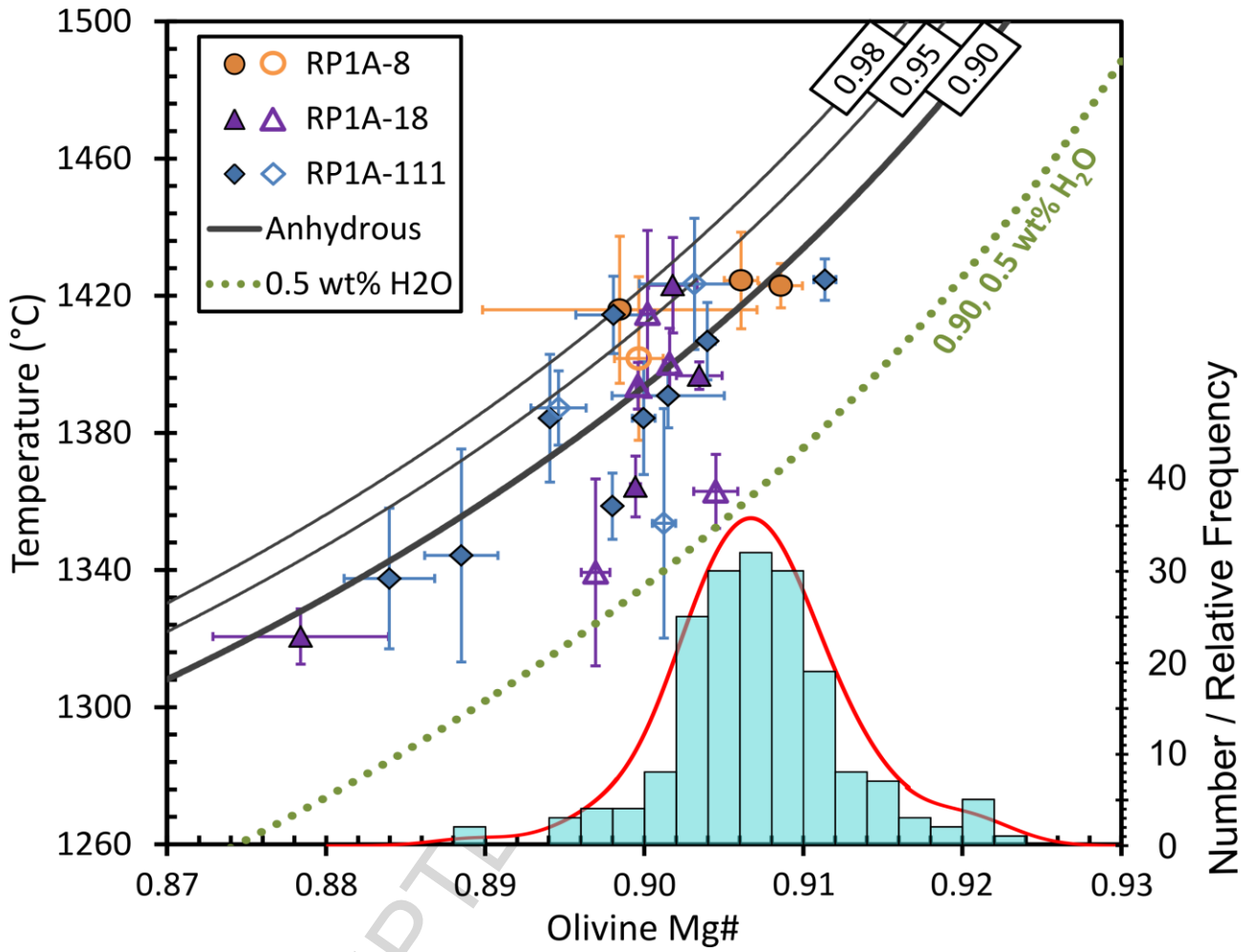


Fig. 8

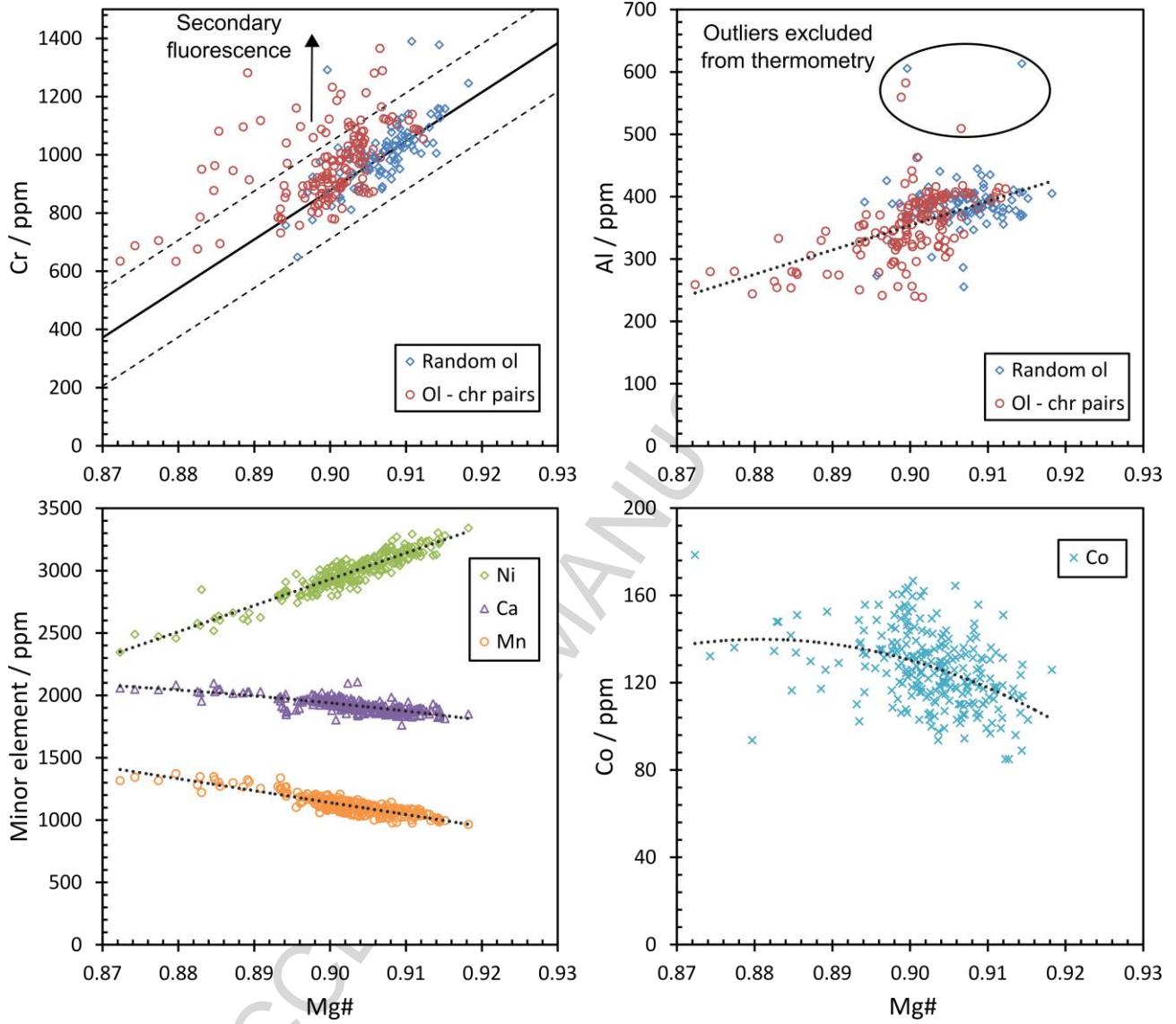


Fig. 9

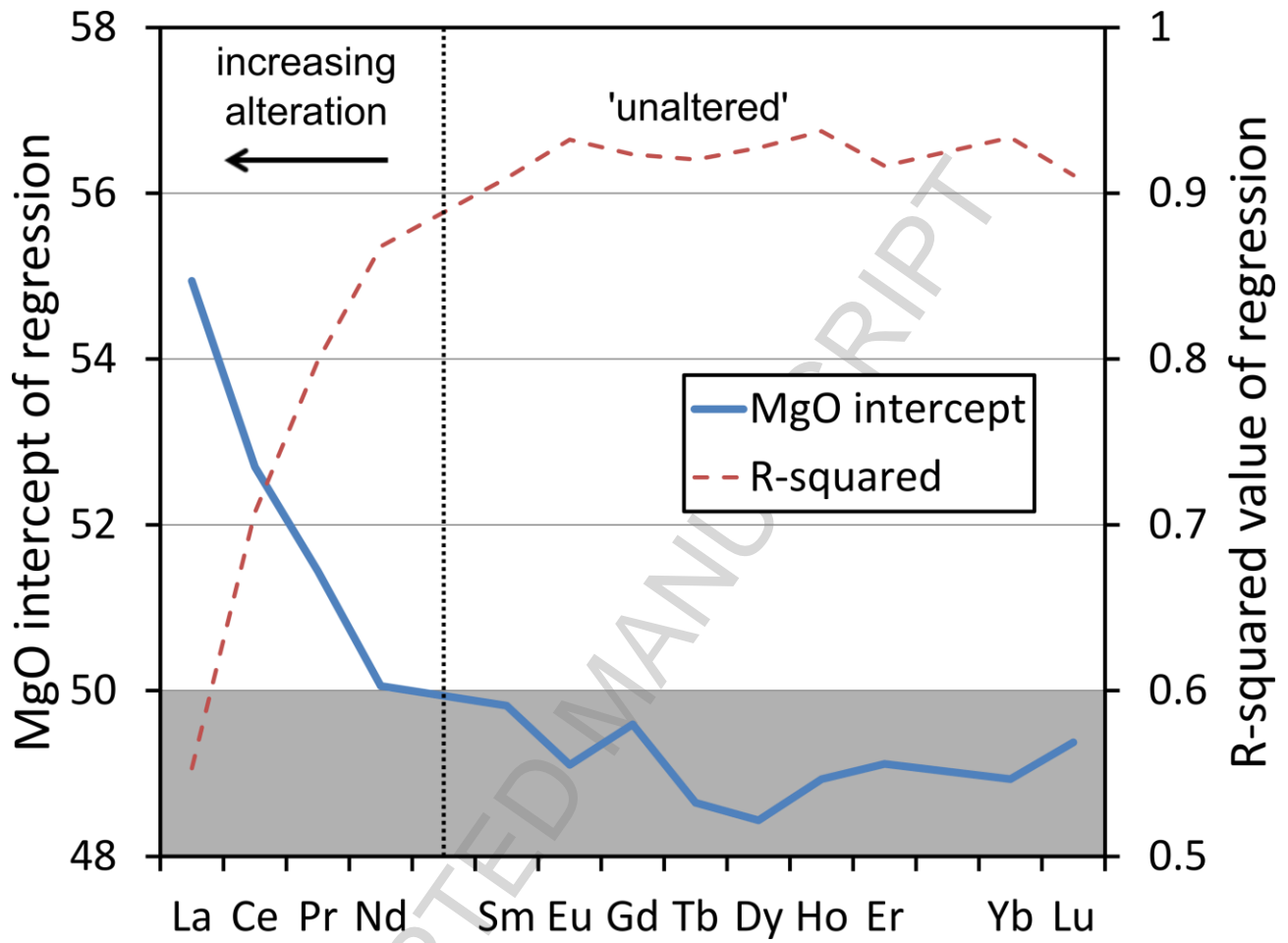


Fig. 10

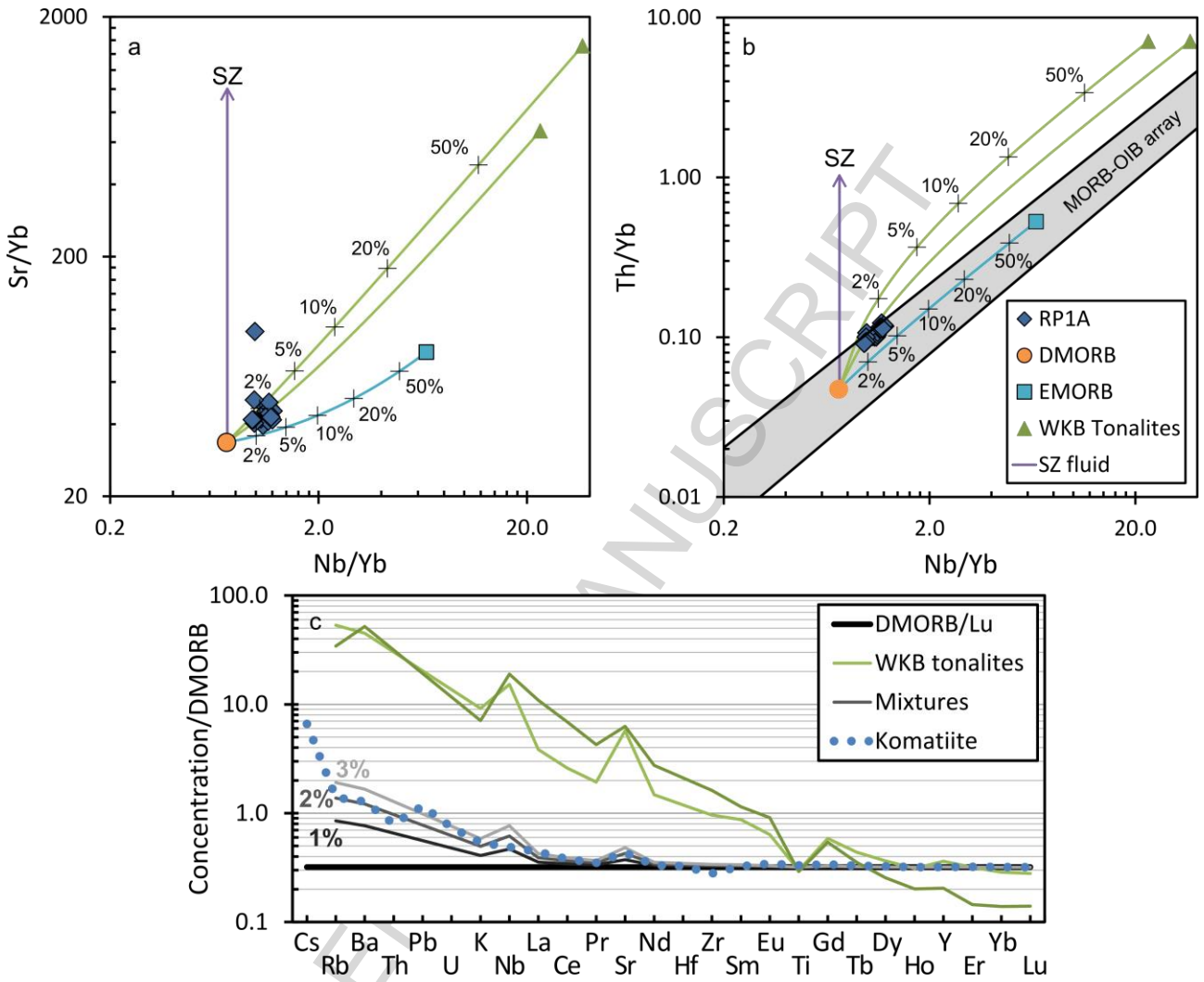


Fig. 11

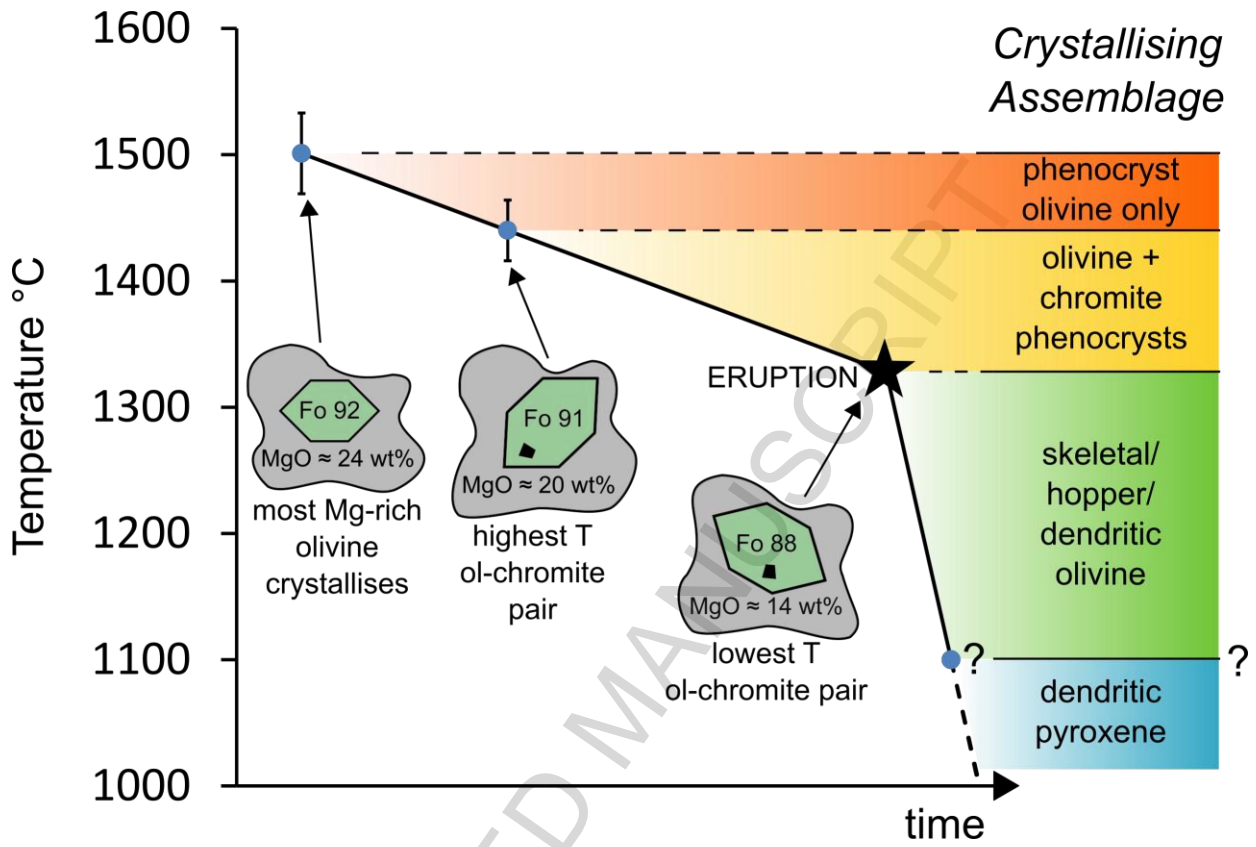


Fig. 12

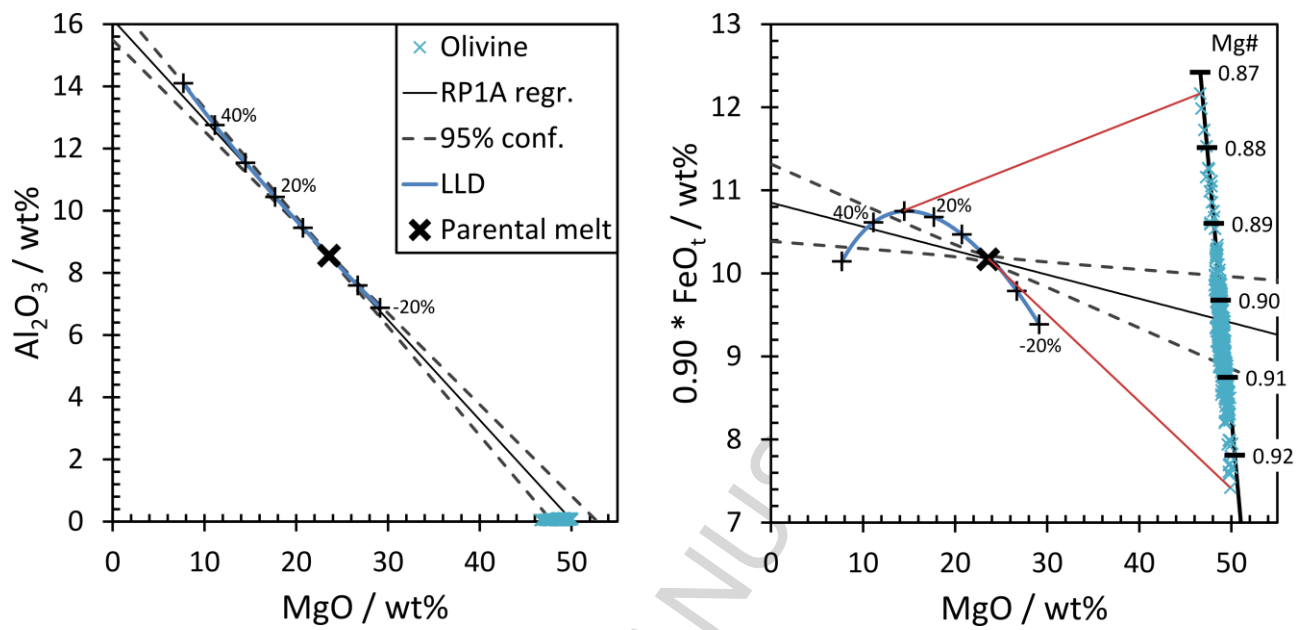


Fig. 13

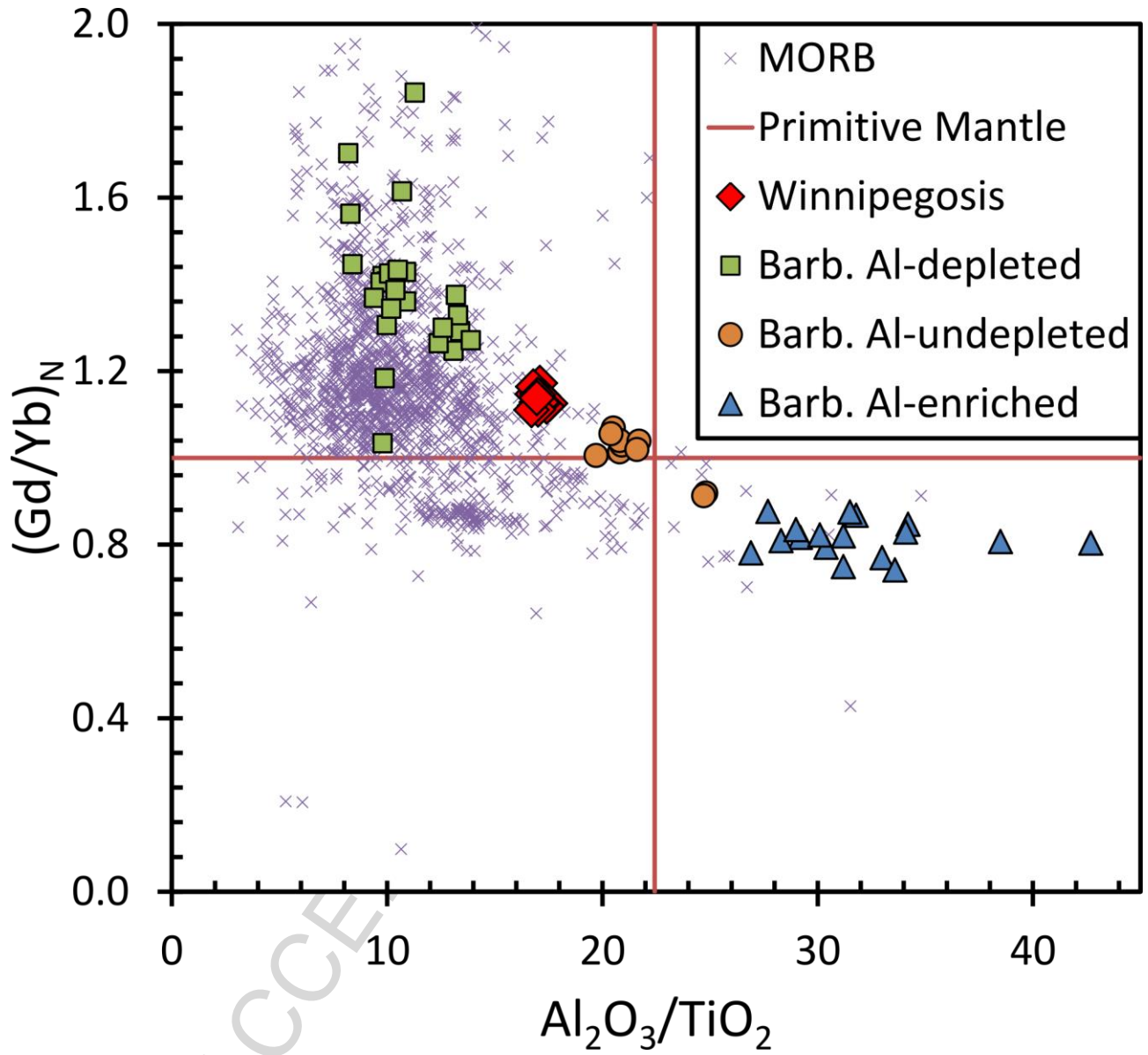
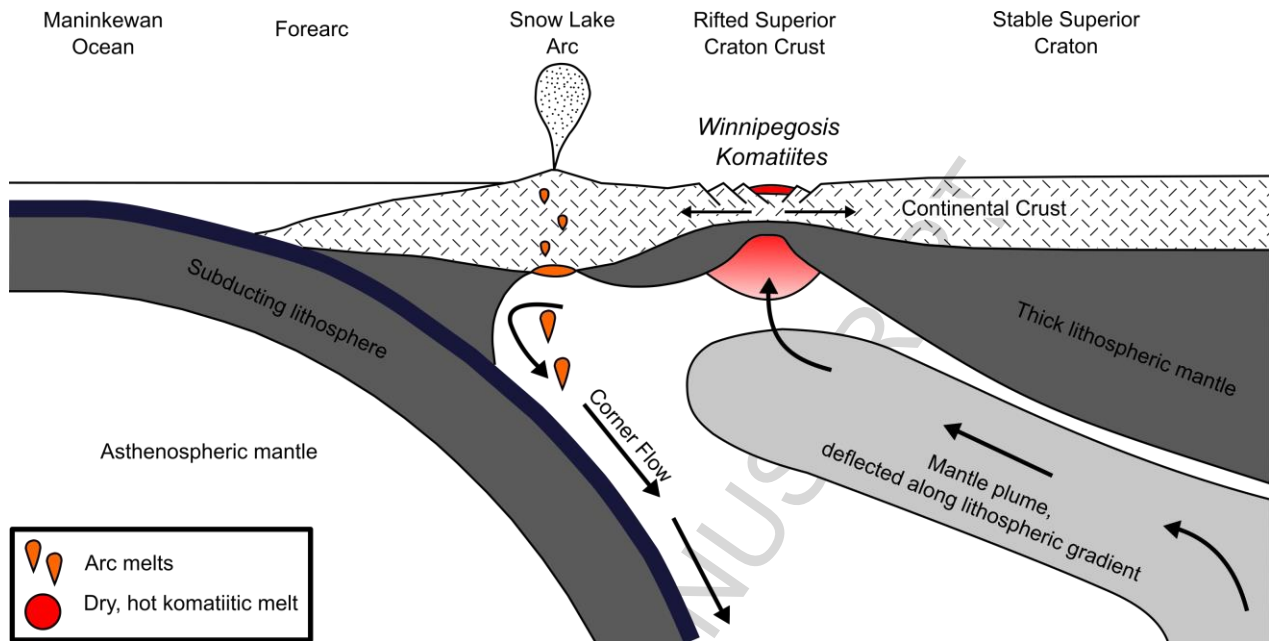
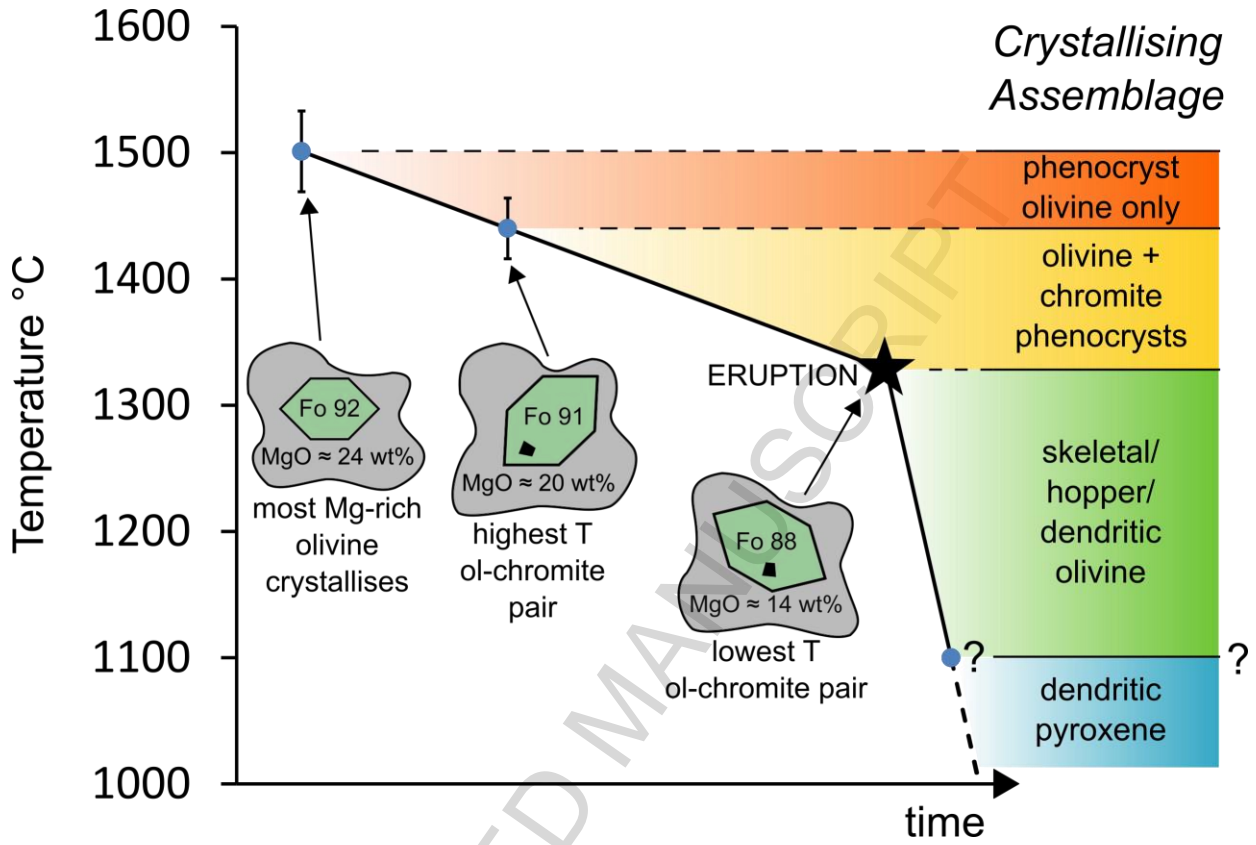


Fig. 14



Graphical abstract



Highlights

- Exceptionally fresh Palaeoproterozoic komatiites are described, and their cooling and crystallisation history is reconstructed
- Parental melts were nominally dry, with depleted compositions, and MgO contents ≈ 24 wt%
- Liquidus temperature of ~ 1501 °C requires anomalously hot mantle
- Proposed formation of the Winnipegosis Komatiites and Circum-Superior Belt from a mantle plume that was deflected by strong gradients in lithospheric thickness towards pre-existing rifts
- New U-Pb zircon age of 1870.3 ± 7.1 Ma for the Winnipegosis Komatiite Belt